ORDER AND CHAOS IN MULTI–DIMENSIONAL HAMILTONIAN SYSTEMS

Tassos BOUNTIS(*), Christos Antonopoulos(*) and Vassileios Basios(**)

(*) Department of Mathematics and Center for Research and Applications of Nonlinear Systems (CRANS), University of Patras, GR–26500, Rion, Patras, Greece

(**) Interdisciplinary Center for Nonlinear Phenomena and Complex Systems (CENOLI), Service de Physique des Systèmes Complexes et Mécanique Statistique, Université Libre de Bruxelles, 1050, Brussels, Belgium

1st Ph.D. School on "Mathematical Modeling of Complex Systems"

Part II

Complex Statistics of Quasistationary Chaotic States in Hamiltonian Systems

Complex Hamiltonian Dynamics

Tassos Bountis and Haris Skokos

Springer Synergetics series 2011

Ch. 1. Fundamental concepts of Lyapunov and Poincare
Ch. 2. Hamiltonian Systems of Few Degrees of Freedom
Ch. 3. Local and Global Stability of Motion
Ch. 4. Normal Modes, Symmetries and Stability
Ch. 5. Efficient Indicators of Stable and Chaotic Motion
Ch. 6. FPU Recurrences and the Transition from Weak to Strong Chaos
Ch. 7. Localization and Diffusion in Nonlinear 1-Dimensional Lattices
Ch. 8. The Statistical Mechanics of Quasi-Stationary States

Contents

Sums of Random Variables and the Central Limit Theorem

The approach we shall follow is in the spirit of the Central Limit Theorem (CLT). In particular, we focus on chaotic regions of: (a) **area–preserving maps**

$$\begin{cases} x_{n+1} = f(x_n, y_n) \\ y_{n+1} = g(x_n, y_n) \end{cases} \tag{1}$$

and (b) N**–degree–of–freedom Hamiltonian systems**

$$\frac{dq_k}{dt} = \frac{\partial H}{\partial p_k}, \quad \frac{dp_k}{dt} = -\frac{\partial H}{\partial q_k}, \quad k = 1, 2, \ldots, N \tag{2}$$

and construct **distributions** of suitably rescaled sums of M values of an observable $\eta_i = \eta(t_i)$ $(i = 1, \ldots, M)$, which is a linear combination of the variables (x_n, y_n), or $(q_n(t), p_n(t))$ of (1) and (2) respectively. These are viewed as **independent random variables** in the limit $M \to \infty$ and we evaluate their sums

$$S_M^{(j)} = \sum_{i=1}^{M} \eta_i^{(j)} \tag{3}$$

where $j = 1, \ldots, N_{\text{ic}}$ refers to different initial conditions. We then study the **probability density functions (pdfs)** of the variables $S_M^{(j)}$, centered about their mean value $\langle S_M^{(j)} \rangle$ and rescaled by their standard deviation σ_M

$$s_M^{(j)} \equiv \frac{1}{\sigma_M}\left(S_M^{(j)} - \langle S_M^{(j)} \rangle\right) = \frac{1}{\sigma_M}\left(\sum_{i=1}^{M} \eta_i^{(j)} - \frac{1}{N_{\text{ic}}} \sum_{j=1}^{N_{\text{ic}}} \sum_{i=1}^{M} \eta_i^{(j)}\right) \tag{4}$$

where

$$\sigma_M^2 = \frac{1}{N_{\text{ic}}} \sum_{j=1}^{N_{\text{ic}}} \left(S_M^{(j)} - \langle S_M^{(j)} \rangle\right)^2 = \langle S_M^{(j)2} \rangle - \langle S_M^{(j)} \rangle^2. \tag{5}$$

If our variables are **random**, or **belong to uniformly ergodic regimes** of deterministic systems, when we plot the normalized distribution of the probabilities $P(s_M^{(j)})$ as a function of $s_M^{(j)}$, , we expect to find in the spirit of the classical CLT:

$$P(s_M^{(j)}) = a e^{-\beta s_M^{(j)2}} \tag{6}$$

i.e a **Gaussian pdf**.

However, as we will show in many examples of **conservative systems**, in regimes of **"weak chaos"**, these distributions are well–approximated by different pdfs, the most ubiquitous of them being the q**-Gaussian**:

$$P(s_M^{(j)}) = a e_q^{-\beta s_M^{(j)2}} \equiv a\left(1-(1-q)\beta s_M^{(j)2}\right)^{\frac{1}{1-q}} \tag{7}$$

where q is the Tsallis entropy index, β is a free parameter and a a normalization constant. Expression (14) is a generalization of the Gaussian, since in the limit $q \to 1$ we have $lim_{q\to 1} e_q^{-\beta x^2} = e^{-\beta x^2}$. If $1 \leq q < 3$, (14) is normalized for an appropriate choice of $a(\beta)$.

As we shall demonstrate, there are **many interesting cases of conservative systems**, where chaotic orbits are strongly influenced by **"stickiness" phenomena** and produce **long–lived quasi–stationary states** (QSS), whose pdfs are well–approximated by q–Gaussians. These, however, frequently **do not converge** to (14), but evolve, through a sequence of QSS, which we seek to identify the limit $t \to \infty$.

Nonextensive Statistical Mechanics and q-Gaussians

Multi–particle systems belong to **different "universality" classes**, according to their thermostatistics. In the most widely studied Boltzmann–Gibbs class, if the system can be at any one of $i = 1, 2, ..., W$ states with probability p_i, its entropy is given by the famous formula

$$S_{BG} = -k \sum_{i=1}^{W} p_i ln p_i \tag{8}$$

where k is Boltzmann's constant, provided, of course,

$$\sum_{i=1}^{W} p_i = 1 \tag{9}$$

The BG entropy satisfies the property of **additivity**, i.e. if A and B are two statistically independent systems, the probability to be in their union is $p_{i,j}^{A+B} = p_i^A p_j^B$ and this necessitates that the entropy of the joint state obeys

$$S_{BG}(A + B) = S_{BG}(A) + S_{BG}(B) \tag{10}$$

At thermal equilibrium, the p_i**s that optimize the BG entropy**, subject to ((9)) and a given energy spectrum E_i and temperature T are:

$$p_i = \frac{e^{-\beta E_i}}{Z_{BG}}, \qquad Z_{BG} = \sum_{i=1}^{W} e^{-\beta E_i} \tag{11}$$

where $\beta = 1/kT$ and Z_{BG} is the so–called partition function. For a continuum set of states depending on one variable, x, the optimal probability density function (pdf) corresponding to BG statistics subject to ((9)), zero mean and given variance V is, of course, the well–known Gaussian $p(x) = e^{-x^2/2V}/\sqrt{2V}$.
Another important property of the BG entropy is that it is **extensive**,

$$lim_{N\to\infty} \frac{S_{BG}}{N} < \infty \tag{12}$$

i.e. it grows **linearly** as a function of with the number of degrees of freedom N of the system.

But then, what about **many physically important systems** that are **not extensive**?

There are **many examples of non–extensive systems**, like: self–gravitating systems of finitely many mass points, interacting black holes, ferromagnetic models, systems with long range forces, in which **strong correlations and power laws** are dominant.

In deterministic dynamics, for instance, **chaos does not always mean exponential instability**, as there are regimes of **"weak chaos"**, where "stickiness phenomena" occur on strange invariant sets near the boundary of regions of regular motion called **'edge of chaos'**, where **Lyapunov exponents are zero** and orbits separate linearly from each other.

It is for these type of situations that Tsallis proposed a different form of entropy [Tsallis,2009]

$$S_q = k\frac{1-\sum_{i=1}^{W} p_i^q}{q-1} \text{ with } \sum_{i=1}^{W} p_i = 1 \qquad (13)$$

depending on an index q, where $i = 1, \ldots, W$ counts the microstates of the system occurring with probability p_i and k is the Boltzmann constant.

Just as the Gaussian distribution represents an **extremal of the BG entropy** ((8)), so is the **q–Gaussian pdf shown below** obtained as a **maximum** (for $q > 0$) or a **minimum** (q<0) of the Tsallis entropy ((13)).

$$p(x) = ae_q^{-\beta x^2} \equiv a\left(1 - (1-q)\beta x^2\right)^{\frac{1}{1-q}} \tag{14}$$

for a continuum set of states.

The Tsallis entropy is **not additive**, as

$$S_q(A+B) = S_q(A) + S_q(B) + k(1-q)S_q(A)S_q(B) \tag{15}$$

and hence **is not extensive**. It thus offers the possibility of studying cases where the A, B subsystems mentioned above are strongly correlated.

Systems characterized by (13) are said to lie at the “edge of chaos” and are significantly different from BG systems.

Pdfs of Chaotic States in Area–Preserving maps

Consider the perturbed MacMillan map, which occurs in the study of equilibrium configurations of Ablowitz–Ladik Discrete Nonlinear Schrodinger Equations:

$$\begin{cases} x_{n+1} = y_n \\ y_{n+1} = -x_n + 2\mu \frac{y_n}{1+y_n^2} + \epsilon y_n \end{cases} \tag{16}$$

with parameters ϵ, μ. Since its Jacobian is 1, (16) is area-preserving.

We have analyzed the histogram of their normalized sums for a range of parameters (ϵ, μ) and have identified some generic classes of q-**Gaussians** and exponentials $\sim e^{-k|z|}$ having a **triangular shape on log scale**, which we call **triangular distributions**. Monitoring their time evolution for increasing number of iterations N, we observe the occurrence of different QSS, which we present with the corresponding phase space plots in the Figures below.

ϵ	0.2	0.5	0.9	1.2	1.6	1.8
L_{max}	0.0867	0.082	0.0875	0.0513	0.0495	0.05876

Table 1: Maximal Lyapunov exponents for $\mu = 0.6$ and $\epsilon = 0.2, 0.5, 0.9, 1.2, 1.6, 1.8$.

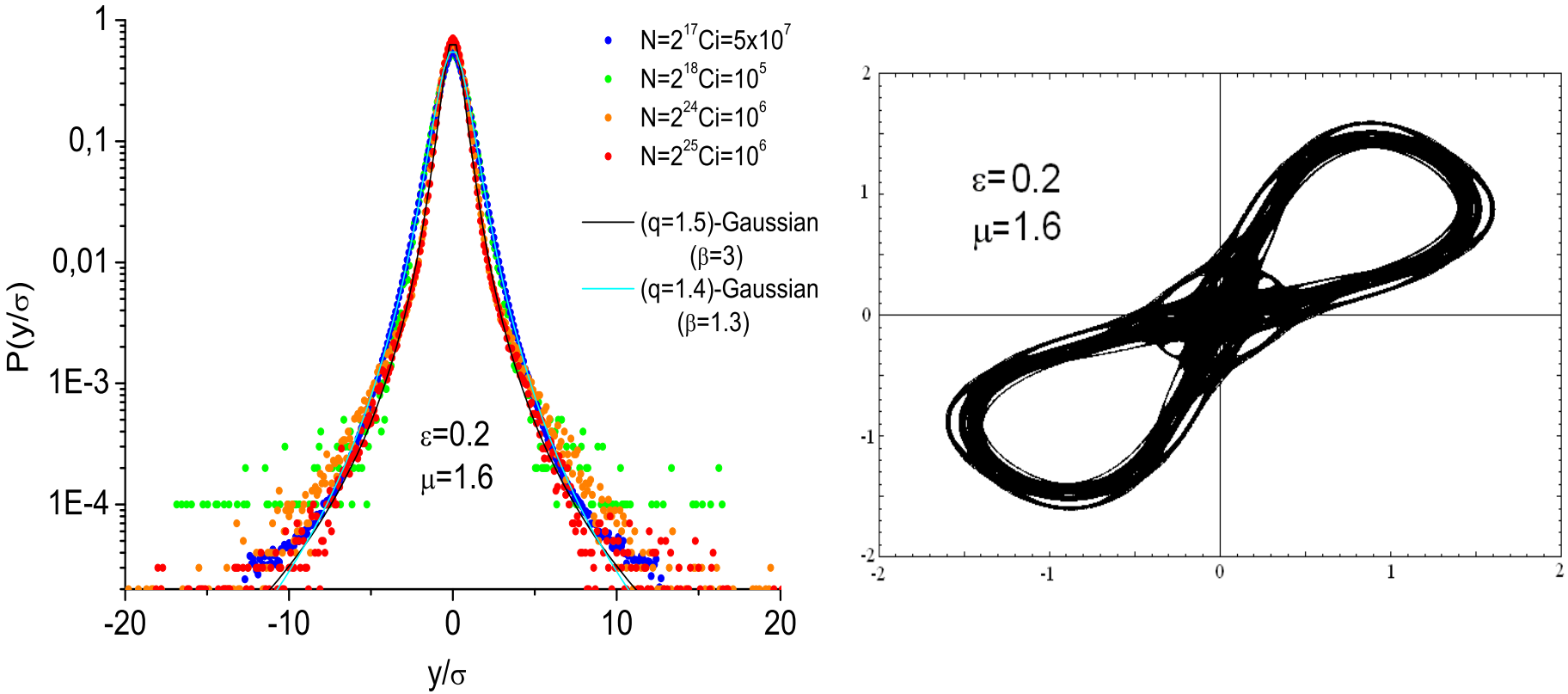

Figure 1. Dynamical and statistical behavior of chaotic orbits of the MacMillan map for parameter values $\mu = 1.6$, and $\epsilon = 0.2$. The first column represents the pdfs of the normalized sums of iterates and the second depicts the corresponding phase space plot. N represents the number of (summed) iterates and N_{ic} is the number of initial conditions that have been randomly chosen from a square $(0, 10^{-6}) \times (0, 10^{-6})$.

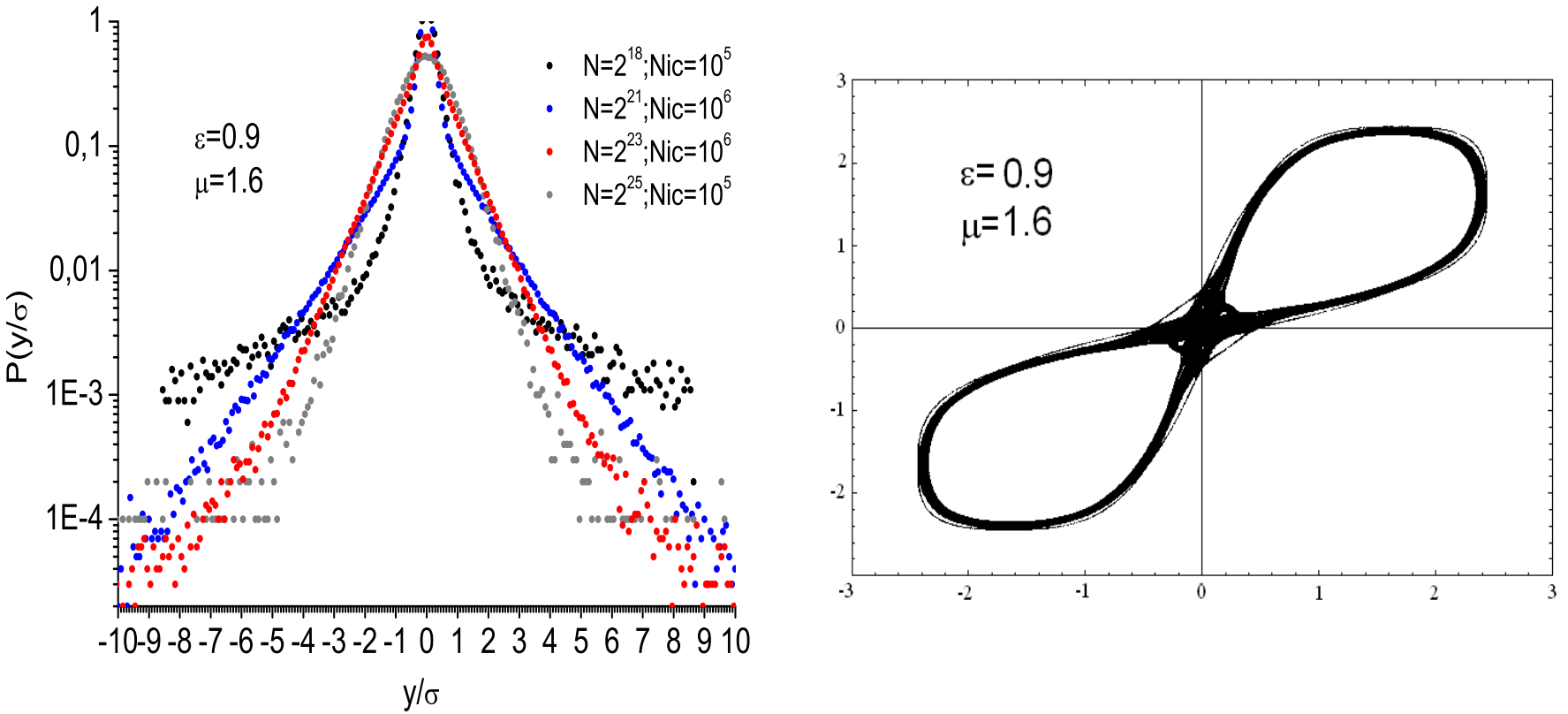

Figure 2. Dynamical and statistical behavior of chaotic orbits of the MacMillan map for parameter values $\mu = 1.6$, and $\epsilon = 0.9$. The first column represents the pdfs of the normalized sums of iterates and the second depicts the corresponding phase space plot. N represents the number of (summed) iterates and N_{ic} is the number of initial conditions that have been randomly chosen from a square $(0, 10^{-6}) \times (0, 10^{-6})$.

A. The $\epsilon = 0.9, 0.2, 1.8$, ($\mu = 1.6$) cases

The $\epsilon = 0.9$ case is a typical example producing time–evolving pdfs. Figures 1 and 2 show that the corresponding phase space plots yield a simple chaotic region in phase space around two islands, yet the corresponding pdfs do not converge to a single distribution, rather they pass from q-**Gaussians** to **triangular** to **Gaussian** distributions.

There exist at least **three long–lived QSS** whose iterates generate pdfs passing through different shapes. Consequently, for $i = 1 \ldots N = 2^{16}$, a QSS is produced whose pdf is a $(q = 1.6)$–Gaussian whose β increases with increasing N. This is not due to a vanishing Lyapunov exponent, but rather to a **"stickiness"** effect around islands of regular motion. In fact, the boundaries of these islands is where the **'edge of chaos'** regime is expected in conservative maps.

Figures 3 and 4 show phase space plots for a number of iterates N. Note that for $N = 1 \ldots 2^{16}$, a 'figure eight' chaotic region is formed around two islands. But for $N > 2^{16}$, a more complex structure emerges, as iterates stick around new islands, and the partial structure of phase space passes through a sequence of quasi-stationary states.

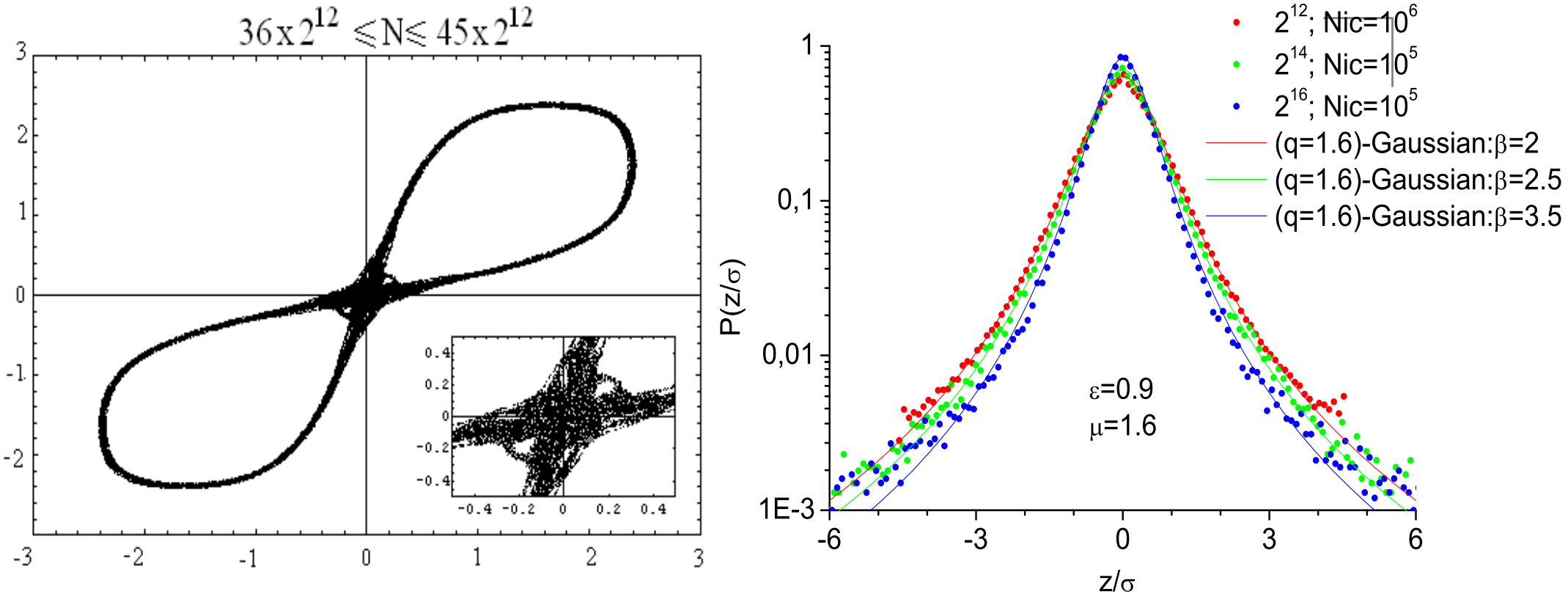

Figure 3. $\epsilon = 0.9$, $\mu = 1.6$ MacMillan map phase space plots (first panel) and the corresponding PDFs (second panel) of the re-normalized sums as the number of iterates $i = 1 \ldots N, N \leq 10^{16}$ increases, starting from a randomly chosen initial condition in a square $(0, 10^{-6}) \times (0, 10^{-6})$.

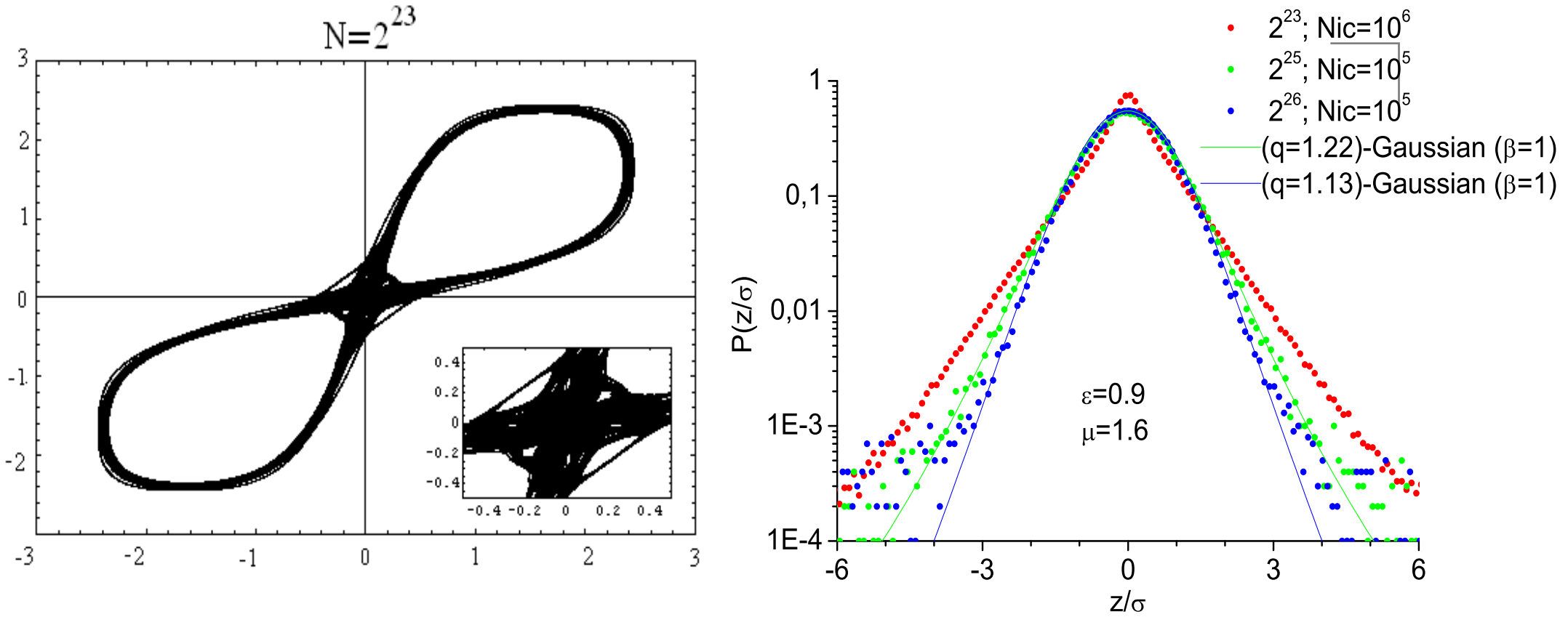

Figure 4. $\epsilon = 0.9$, $\mu = 1.6$ MacMillan map phase space for $i = 1 \ldots N, N \geq 2^{23}$ plot iterates, starting from a randomly chosen initial condition in a square $(0, 10^{-6}) \times (0, 10^{-6})$ and the corresponding pdfs (right panel).

Thus, more than one QSS coexist whose pdfs are the superposition of their corresponding $(q \neq 1)$–Gaussians. In fact, note in Figure 3 that this superposition of QSS for $N \leq 2^{21}$ produces a distribution where central part is still well–described by a $(q = 1.6)$**–Gaussian**.

However, as we continue to iterate the map to $N = 2^{23}$, this $(q = 1.6)$–Gaussian passes through a superposition of states characterized by **triangular distributions**. From here on, as $N > 2^{23}$, the central part of the pdfs become q–Gaussians with $q \to 1$ (see Figure 4) and a true **Gaussian** is expected in the limit ($N \to \infty$).

B. The $\epsilon = 1.2, 1.6$, ($\mu = 1.6$) cases

Let us now analyze the cases $\epsilon = 1.2$, whose maximum Lyapunov exponent is $L_{max} \approx 0.05$. In Figure 5 iterates show a **diffusive behavior** that spreads around islands of a higher order resonance, as iterations reach $N = 2^{19}$.

The central part of the pdfs attains a $(q = 1.6)$**–Gaussian** for $N \leq 2^{16}$ (left panel of Fig. 5). Then, orbits diffuse outward and even the tail of the pdf converges to a $(q = 1.6)$-Gaussian (right panel of Fig. 5). For larger N, diffusion ceases at the q–Gaussian of Figure 6.

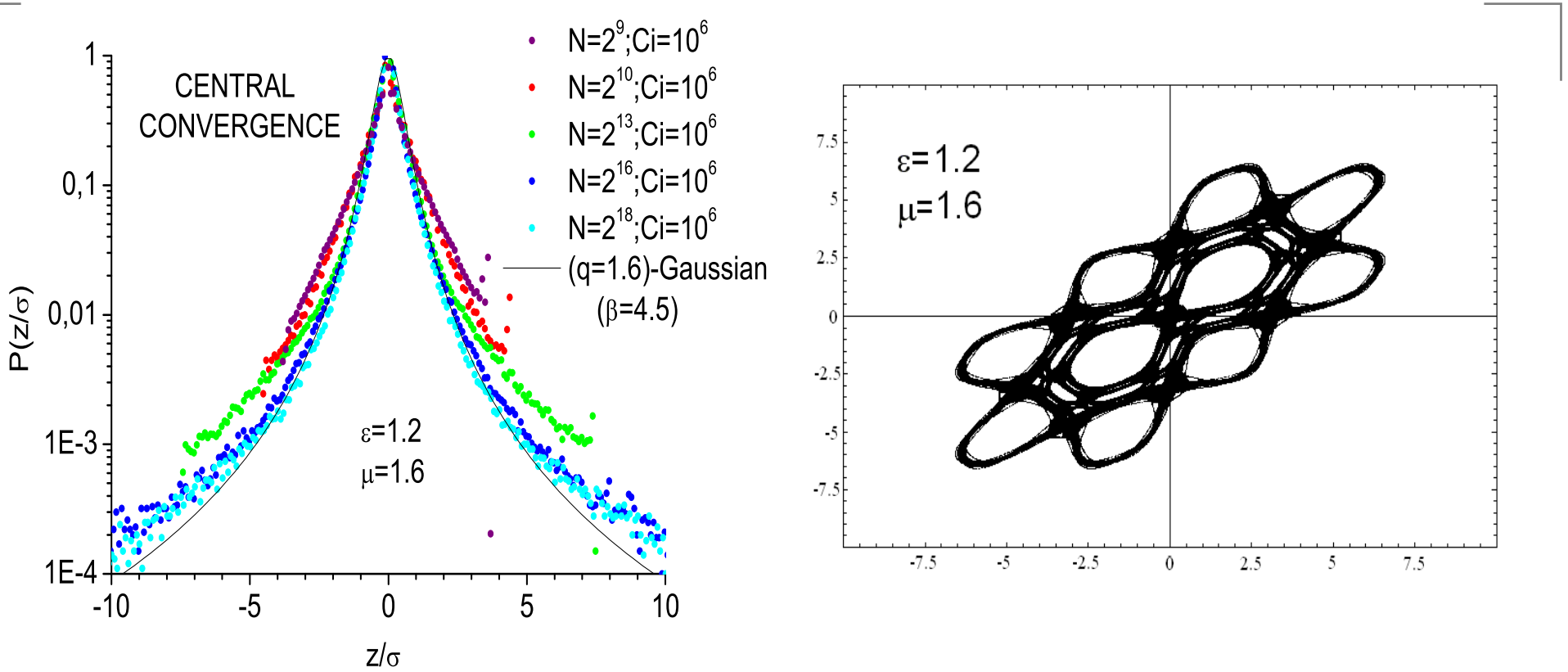

Figure 5. Dynamical and statistical behavior of chaotic orbits of the MacMillan map for $\mu = 1.6$, and $\epsilon = 1.2$. The right panel depicts the corresponding phase space plot and the left panel shows the pdfs of the normalized sums of iterates. N represents the number of (summed) iterates and N_{ic} is the number of initial conditions that have been randomly chosen from a square $(0, 10^{-6}) \times (0, 10^{-6})$.

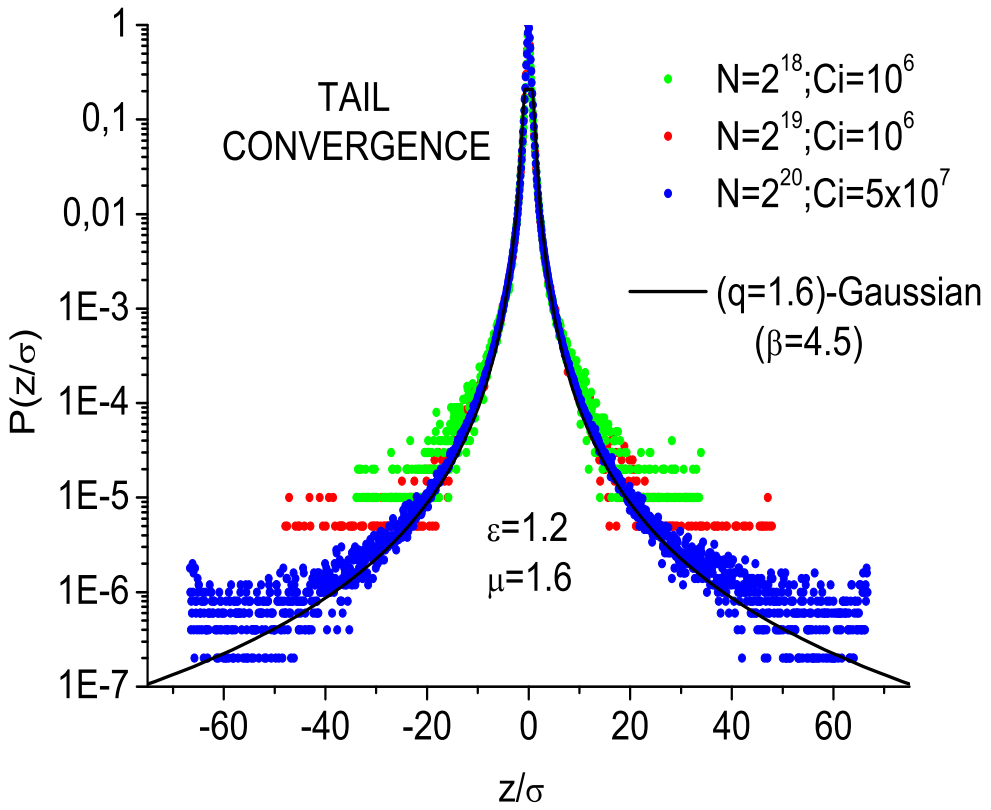

Figure 6. Tail convergence of the q–Gaussian for $\mu = 1.6$, and $\epsilon = 1.2$ depicting the pdfs for $N > 2^{18}$ numbers of iterates.

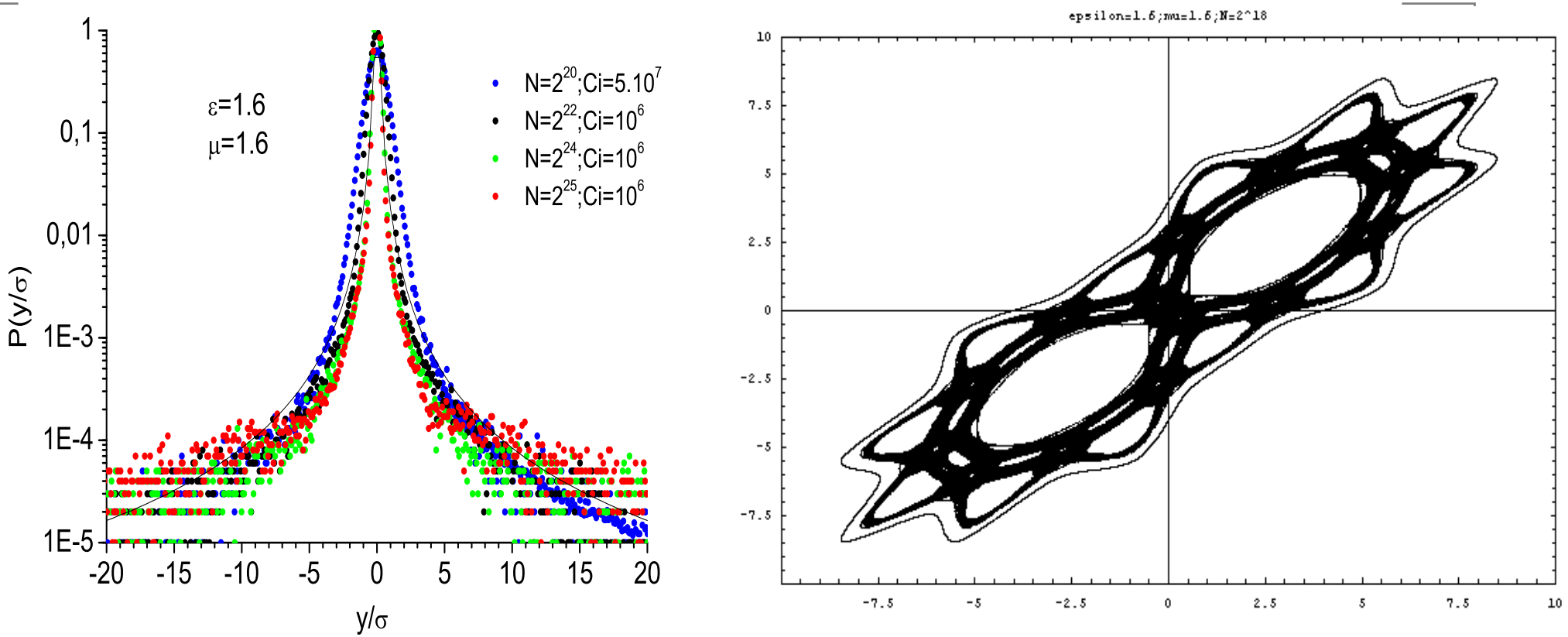

Figure 7. Similar dynamical and statistical behavior of chaotic orbits of the MacMillan map is observed for $\mu = 1.6$, $\epsilon = 1.6$, as in the $\epsilon = 1.2$ case. Orbital diffusion to an outer chain of islands generates pdfs of iterate sums that also converge to a true q–Gaussian as N increases to larger and larger values.

Quasi–stationary Chaotic States in Fermi–Pasta–Ulam Hamiltonians

The FPU $\beta-$ model is a one–dimensional lattice of nonlinear oscillators described by the Hamiltonian

$$H = \frac{1}{2}\sum_{j=1}^{N} p_j^2 + \sum_{j=0}^{N}\left(\frac{1}{2}(q_{j+1}-q_j)^2 + \frac{1}{4}\beta(q_{j+1}-q_j)^4\right) = E \qquad (17)$$

E being its total energy. We shall impose **fixed boundary conditions (fbc)**:
$q_0(t) = q_{N+1}(t) = 0$, or **periodic boundary conditions (pbc)**
$q_j(t) = q_{j+N}(t), \quad p_j(t) = p_{j+N}(t)$, for all $t > 0$.

We focus on **Simple Periodic Orbits (SPOs)**, where all variables oscillate in or out of phase and return to their initial state after only one maximum and one minimum in their oscillation. Examples of such SPOs are **Nonlinear Normal Modes (NNMs)**, i.e. continuations of linear normal modes of the FPU chain described by the Q_q and P_q variables:

$$Q_q = \sqrt{\frac{2}{N+1}}\sum_{i=1}^{N} q_i \sin\frac{qi\pi}{N+1}, \qquad P_q = \dot{Q}_q \qquad (18)$$

These solutions are:

(a) The FPU π–Mode under pbc with N even

$$\hat{q}_j(t) = -\hat{q}_{j+1}(t) \equiv q(t),\ j = 1, \ldots, N \tag{19}$$

(b) The SPO1 mode under fbc, with N odd,

$$\hat{q}_{2j}(t) = 0,\ \hat{q}_{2j-1}(t) = -\hat{q}_{2j+1}(t) \equiv \hat{q}(t),\ j = 1, \ldots, \frac{N-1}{2}. \tag{20}$$

(c) The SPO2 mode under fbc, with $N = 5 + 3m,\ m = 0, 1, 2, \ldots$

$$\hat{q}_{3j}(t) = 0,\ j = 1, 2, 3 \ldots, \frac{N-2}{3}, \tag{21}$$

$$\hat{q}_j(t) = -\hat{q}_{j+1}(t) = \hat{q}(t),\ j = 1, 4, 7, \ldots, N-1. \tag{22}$$

which are exact continuations of the $q = N/2$, $q = (N+1)/2$ and $q = 2(N+1)/3$ linear modes respectively. Let us see what these solutions look like for some small particle chains.

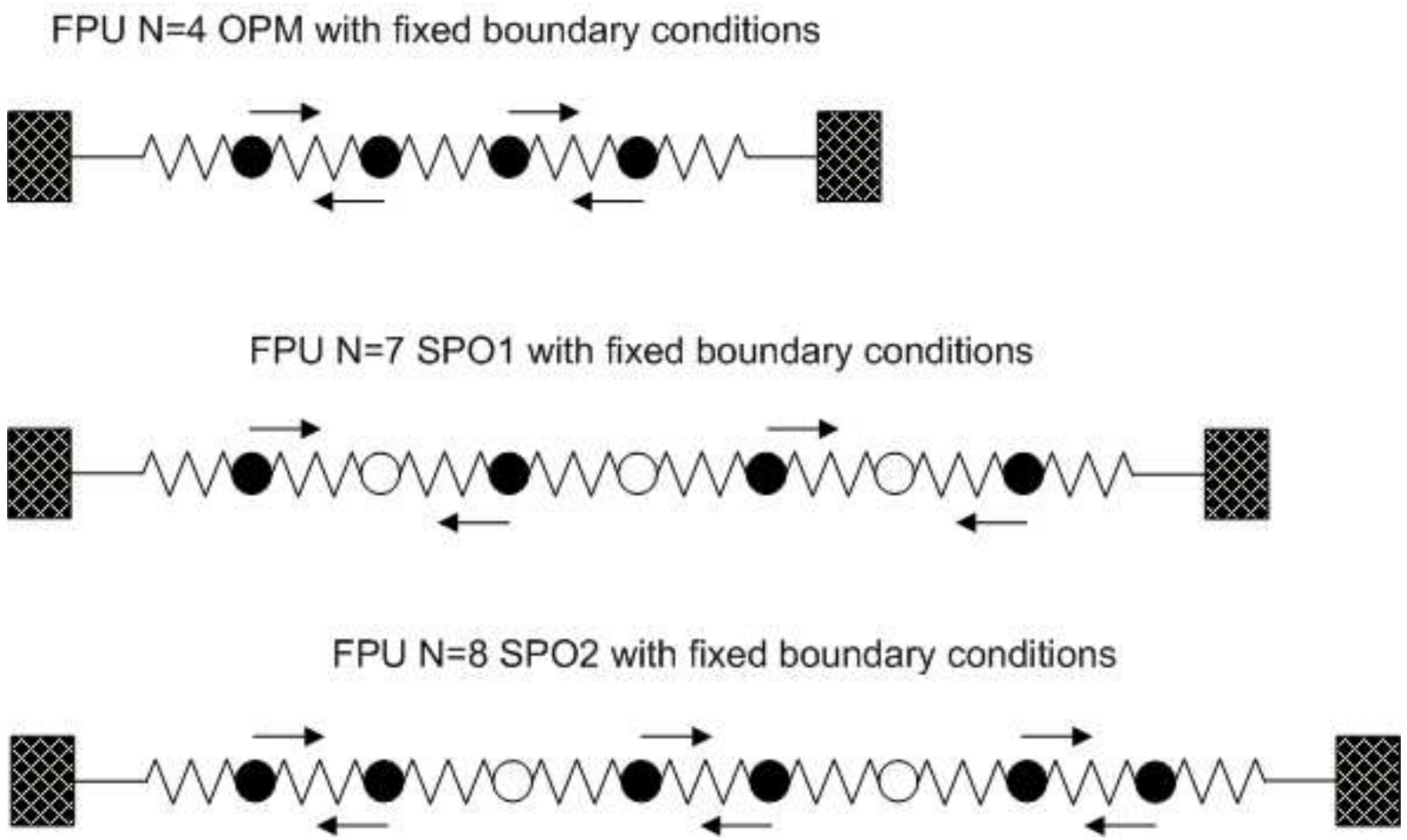

Figure 8: The π–mode of oppositely moving particles, the SPO1 mode corresponding to every other particle being stationary and the SPO2 mode, with one stationary particle every other two.

First, we specify an observable denoted by $\eta(t)$ in terms of one (or more) of the components of a chaotic solution, which visits all parts of our QSS during the time interval $0 \leq t \leq t_f$. We divide t_f into N_{ic} **equally spaced, consecutive windows**, which are long enough to contain a significant part of the orbit. Next, we subdivide each window into a sufficiently **large number M of equally spaced subintervals** and calculate the sum $S_M^{(j)}$ of the values of the observable $\eta(t)$ at the right edges of these subintervals.

We repeat this process N_{ic} times, to obtain a large number of sums for **reliable statistics**. Next, we compute the average of these sums and their standard deviation, as we already explained in the CLT section, see (4) and (5).

$$\langle S_M^{(j)} \rangle = \frac{1}{N_{\text{ic}}} \sum_{j=1}^{N_{\text{ic}}} S_M^{(j)}, \; \sigma_M = \sqrt{\frac{1}{N_{\text{ic}}} \sum_{j=1}^{N_{\text{ic}}} \left(S_M^{(j)} - \langle S_M^{(j)} \rangle \right)^2} \tag{23}$$

Having all this information, we then proceed to compute the N_{ic} rescaled quantities $s_M^{(j)}$ and plot the histogram $P(s_M^{(j)})$ of their distribution.

Our aim is to study chaotic regions near these NNM orbits, when they have just turned unstable.

(a) The FPU π–Mode under pbc with N even
Here, we choose as an observable the quantity

$$\eta(t) = q_{\frac{N}{2}}(t) + q_{\frac{N}{2}-1}(t) \tag{24}$$

using the fact that $\eta(t) = 0$ and **remains close to zero** at energy values E where the π–mode is still stable. At energies above its first destabilization threshold, i.e. $E > E_u^1$, however, $\eta(t)$ eventually deviates from zero. Following a similar study published recently in [Leo,Leo and Tempesta, 2010], we consider the case of $N = 128$ and $\beta = 1$ for which $E_u^1 \approx 0.0257$ and take as our total energy $E = 0.768$, at which the π–mode is unstable.

As we see in Figures 9 and 10, when we increase the total integration time of our numerical trajectory, the statistical distributions (red curves) approaching **closer and closer to a Gaussian** with q tending to 1. Moreover, the above results seem to be independent of the values of N_{ic} and/or M, at least up to the final integration time $t_f = 10^8$ that we have been able to check.

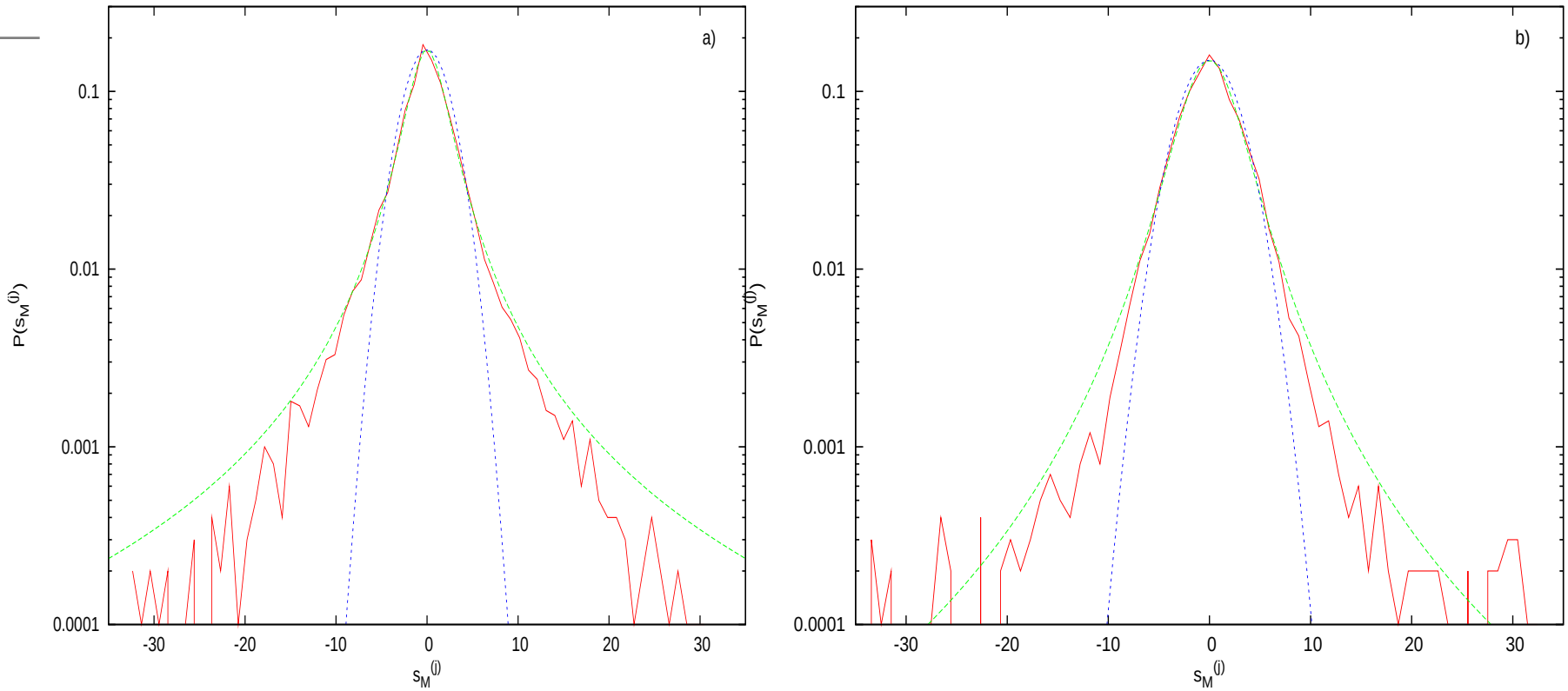

Figure 9. Plot in linear–log scale of numerical (red curve), q–Gaussian (green curve) and Gaussian (blue curve) distributions for the FPU $\pi-$ mode with p.b.c. for $N = 128$ degrees of freedom, $\beta = 1$ and $E = 0.768$. Panel a) corresponds to integration **time** $t_f = 10^5$ using $N_{\text{ic}} = 10$ and $M = 10$ terms in the sums. The numerical fitting with a **q–Gaussian gives** $q \approx 1.818$ with $\chi^2 \approx 0.00070$. Panel b) corresponds to $t_f = 10^6$ using $N_{\text{ic}} = 100$ and $M = 100$ terms in the sums. Here the fitting is with a **q–Gaussian with** $q \approx 1.531$ and $\chi^2 \approx 0.00039$.

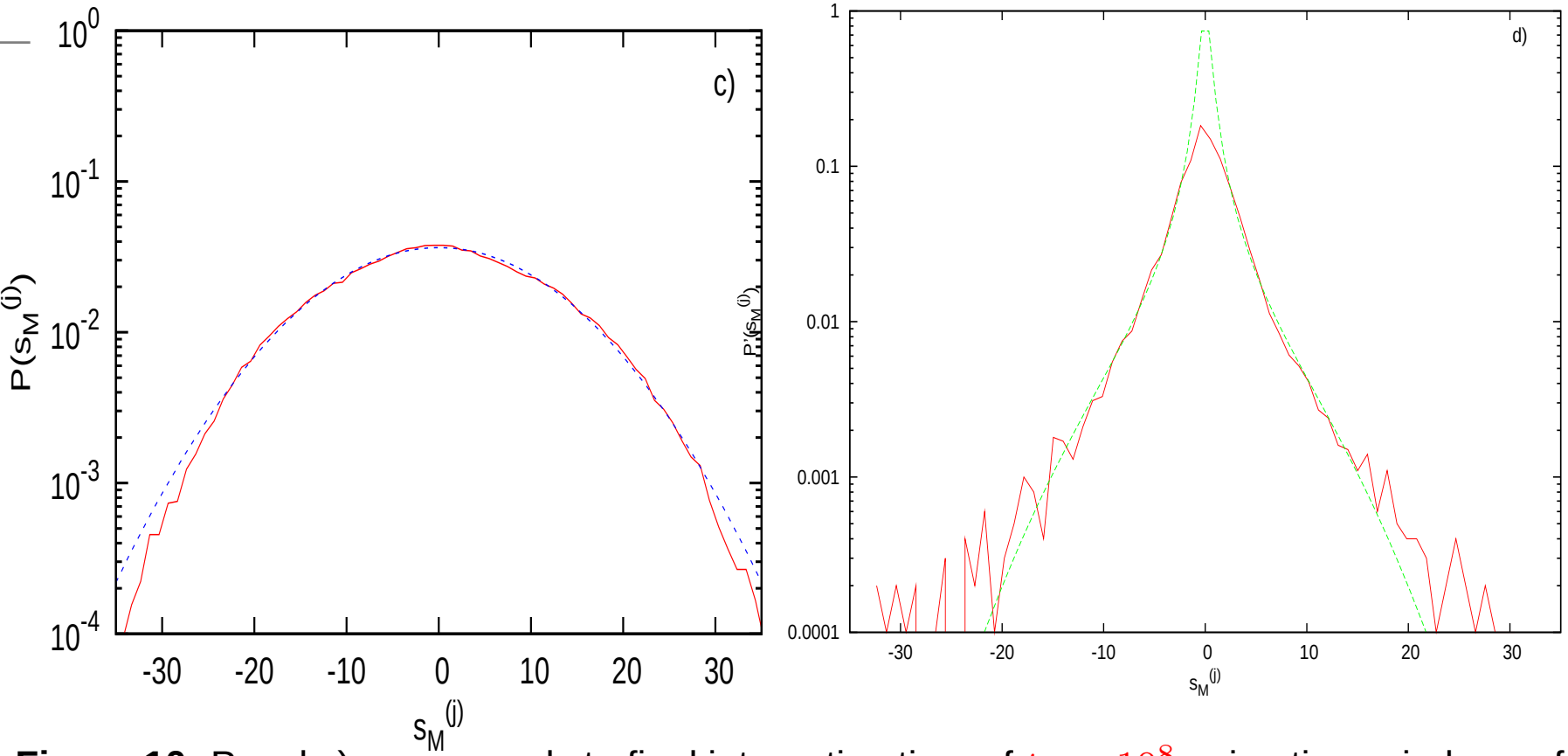

Figure 10. Panel c) corresponds to final integration time of $t_f = 10^8$ using time windows of length $N_{\text{ic}} = 1000$ and $M = 1000$ terms in the computations of the sums. Here the numerical distribution (red curve) has almost converged to a Gaussian (blue curve). Panel d) Plot in linear–log scale of the same numerical distribution as in panel a) (red curve) and of **the P' function of Eq.** (25) for $a_1 \approx 0.009, a_q \approx 2.849$ and $q \approx 2.179$ with $\chi^2 \approx 0.00008$ (green curve). The fitting by this function is evidently better than that with a q–Gaussian.

As Figure 10 (d) shows, the computed distribution (red curve) on its way to a Gaussian, may pass through intermediate QSS, where it is better fitted by a function presented in [Tsallis and Tirnakli, 2010]

$$P'(s_M^{(j)}) = \frac{1}{\left(1 - \frac{a_q}{a_1} + \frac{a_q}{a_1} e^{(q-1)a_1 s_M^{(j)2}}\right)^{\frac{1}{q-1}}}, \; a_1, a_q \geq 0 \text{ and } q > 1 \qquad (25)$$

where $a_1 \approx 0.009, a_q \approx 2.849$ and $q \approx 2.179$ getting $\chi^2 \approx 0.00008$ (in contrast to the $\chi^2 \approx 0.00070$ of a q–Gaussian (14) fitting with $q \approx 1.818$). Eq. (25) contains q–Gaussians in the limit of q being close to 1.

(b) FPU SPO1 mode under fbc

Let us now pass to the second example we consider in this study and examine the chaotic dynamics near another NNM of the FPU system, imposing this time **fixed boundary conditions**. In particular, we study statistical distributions of chaotic orbits in the neighborhood of a nonlinear mode we have called SPO1.

More specifically, we consider the FPU–β one–dimensional lattice of $N = 5$ particles under fbc.

The chaotic regions near this solution (when it has just become unstable) are embedded into each other, as shown in Figure 11. At first, **a "figure eight"** appears created by an orbit starting at a distance $\approx 1.192 \times 10^{-7}$ from the SPO1 mode, see the surface of section (q_1, p_1) of Figure 11 (at times when $q_3 = 0$ and $E = 7.4$).

Orbits starting in the neighborhood of this point remain nearby for very long times, forming the "figure eight" at the middle of the picture. Starting, however, at a distance $\approx 1.086 \times 10^{-2}$ from the saddle point, a **more extended chaotic region** is observed, in the form of a small "figure eight cloud" enveloping the first orbit.

Choosing even more distant initial conditions, e.g. one starting $\approx 3.421 \times 10^{-1}$ from the saddle point, a **much larger chaotic region** is obtained, which spreads uniformly over a much larger part of the available energy surface.

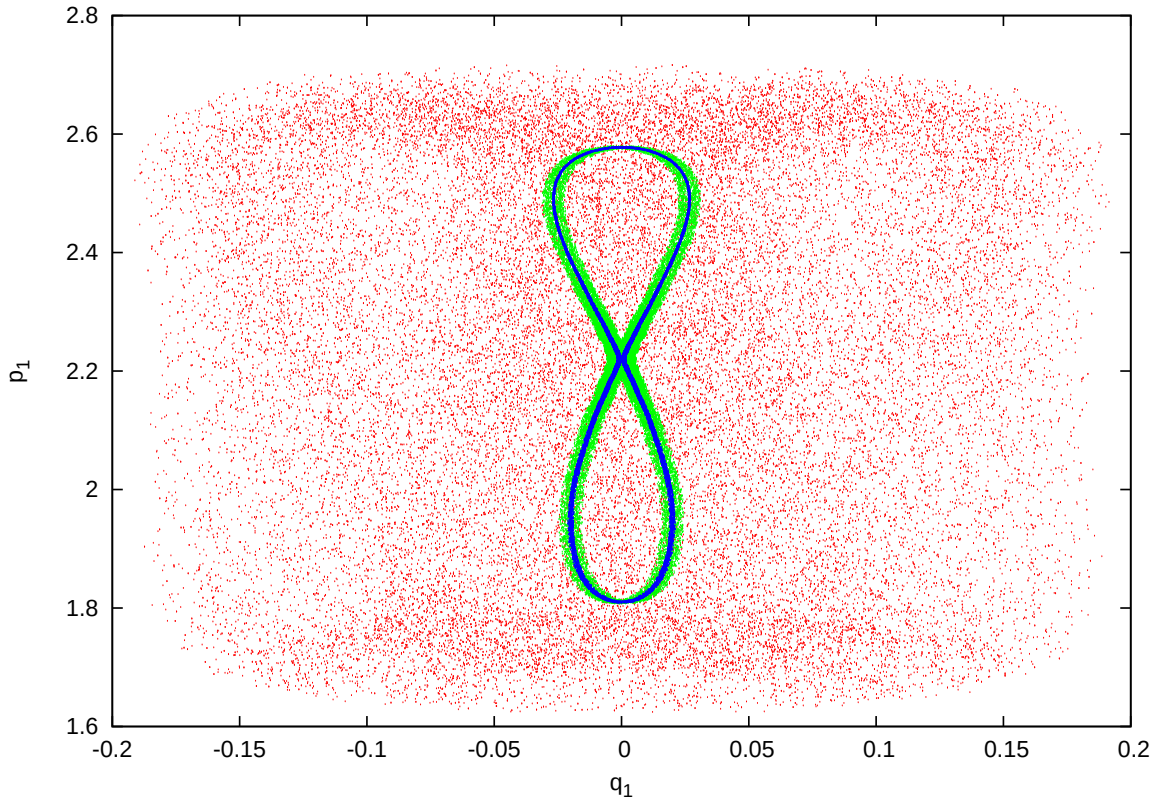

Figure 11: (i) The "figure eight" chaotic region (blue points) for an orbit starting at a distance $\approx 1.192 \times 10^{-7}$ from SPO1 mode at the saddle point in the figure), (ii) a fatter "figure eight cloud" (green points) is seen starting at ($\approx 1.086 \times 10^{-2}$) and a much larger chaotic region (red points) on the energy surface for an initial condition even more distant ($\approx 3.421 \times 10^{-1}$). $N = 5$ and $\beta = 1$, on the surface of section (q_1, p_1) computed at $q_3 = 0$. In this figure, we have integrated our three orbits up to $t_f = 10^5$ on the energy surface $E = 7.4$.

In the present example, we have chosen as an observable the quantity

$$\eta(t) = q_1(t) + q_3(t) \tag{26}$$

which is exactly equal to zero at the SPO1 orbit. In fact, $\eta(t)$ remains very close to zero at energies where the SPO1 mode is stable and becomes nonzero due to numerical errors at energies just above the first destabilization energy E_u^1 of the mode.

We now study the 3 different initial conditions located on the neighborhood of the unstable SPO1 mode (see Fig. 11). In particular, in Figures 12, 13 and 14, we see on the left panel the surface of section created by the trajectory at initial distance $\approx 1.192 \times 10^{-7}$ from the unstable SPO1 integrated up to times $t_f = 10^5$, $t_f = 10^7$ and $t_f = 10^8$ respectively, while on the right panels of these figures we plot the corresponding pfds of the normalized sums.

Clearly, as the integration time t_f grows, our chaotic orbit eventually wanders over a more extended domain, covering gradually a much larger part of the energy surface when $t_f = 10^8$. This may also be explained by the behavior of the Lyapunov exponents of the orbit (see Figure 15).

An important question arises now:

Are these different dynamical behaviors reflected by the normalized sum pdfs and for what integration times? The answer to this question is presented, for an initial distance$1.192E-07$ and for integration time $t_f = 10^5$ in Figure 12(b). Here, a fitting with the **q–Gaussian** (14) **gives** $q \approx 2.785$ with $\chi^2 \approx 0.00031$.

If we now increase the time to $t_f = 10^7$ (see Figure 13(b)) using $N_{\text{ic}} = 100$ and $M = 1000$ terms in the sums and perform the same kind of fit we find a **q–Gaussian fit with** $q \approx 2.483$ and $\chi^2 \approx 0.00047$. This distribution corresponds to the surface of section of Figure 13(a), which shows that in this time the orbit has diffused further in phase space, creating a "fatter" figure eight.

However, the lower parts (tails) of the red distribution are **not fitted well at all by a q–Gaussian**. This suggests that the pdf passes through a transient form, that may well be approximated by other types of functions like (25) mentioned above.

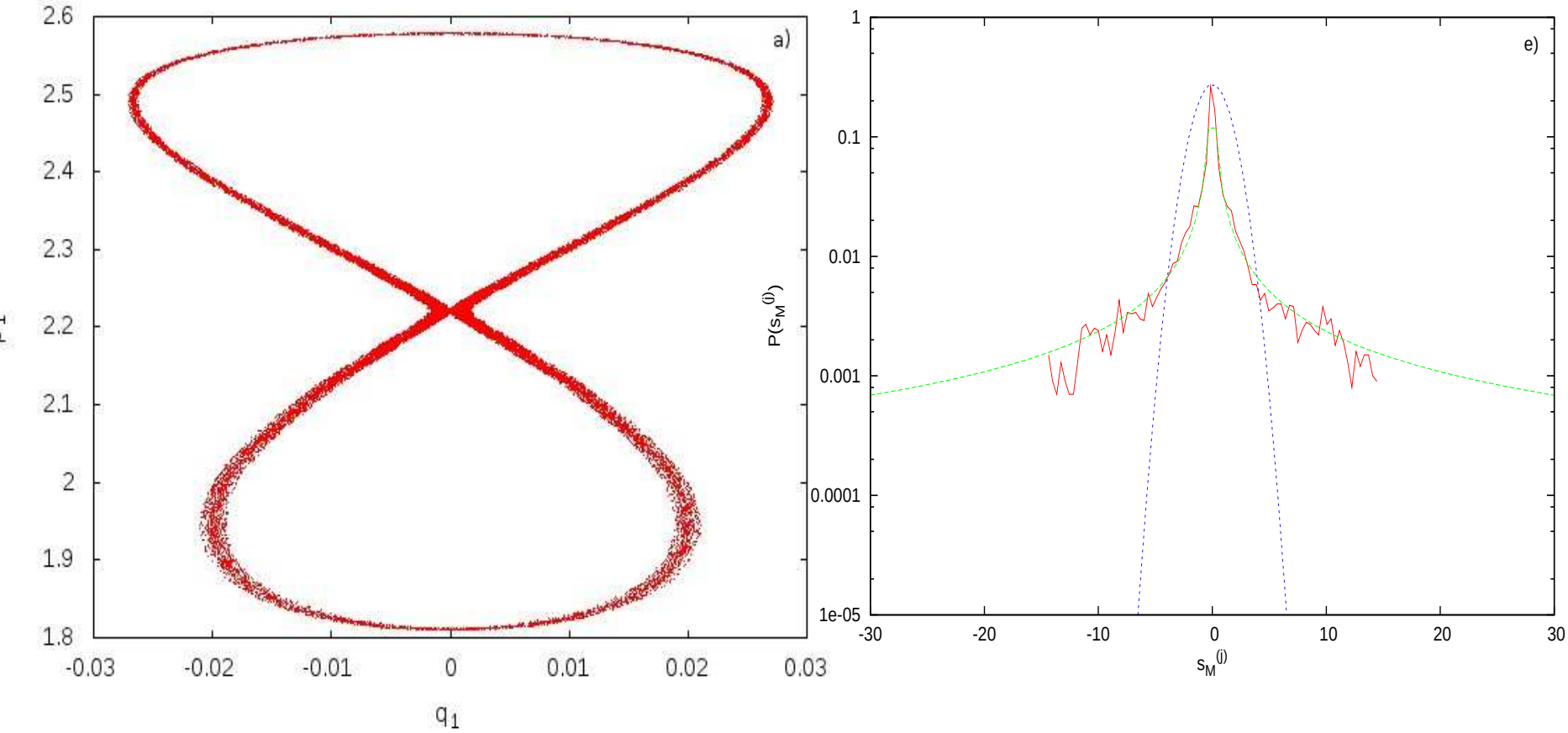

Figure 12. Left: Surface of section of a trajectory starting from a distance of $\approx 1.192 \times 10^{-7}$ from the unstable SPO1 saddle and integrated for **a total time** $t_f = 10^5$. **Right:** For the same integration time, we find that the pdf representing the **distribution of the sums** is well fitted by a q**–Gaussian,** $q \approx 2.785$ with $\chi^2 \approx 4.05 \times 10^{-6}$.

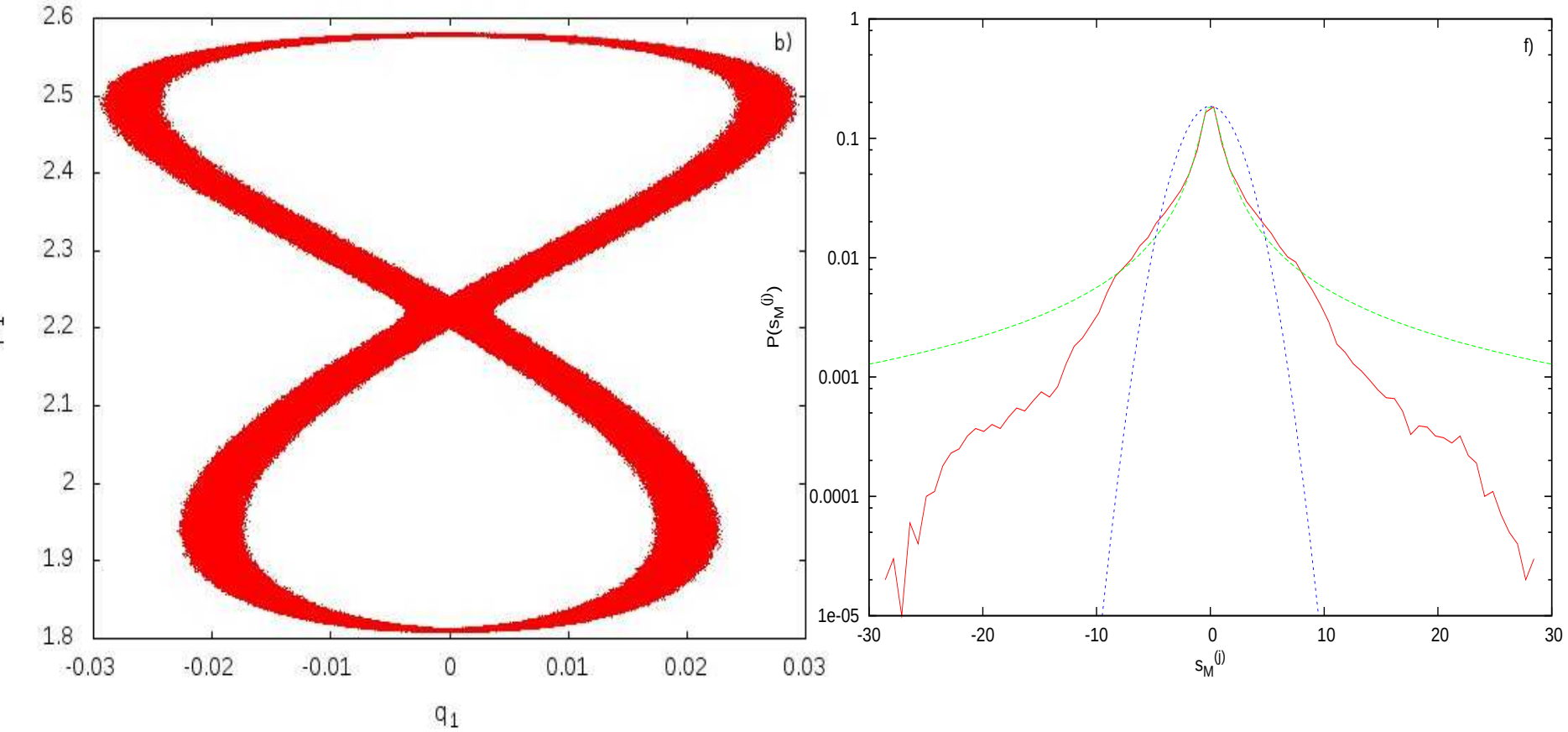

Figure 13: Left: Surface of section of a trajectory starting from an distance $\approx 1.192 \times 10^{-7}$ from the unstable SPO1 saddle point total after time $t_f = 10^7$. **Right:** For the same integration time, the **statistical distribution of the sums** of one chaotic component of the orbit can still be fitted–but not as well–by a q**–Gaussian with** $q \approx 2.483$ with $\chi^2 \approx 6.05 \times 10^{-6}$.

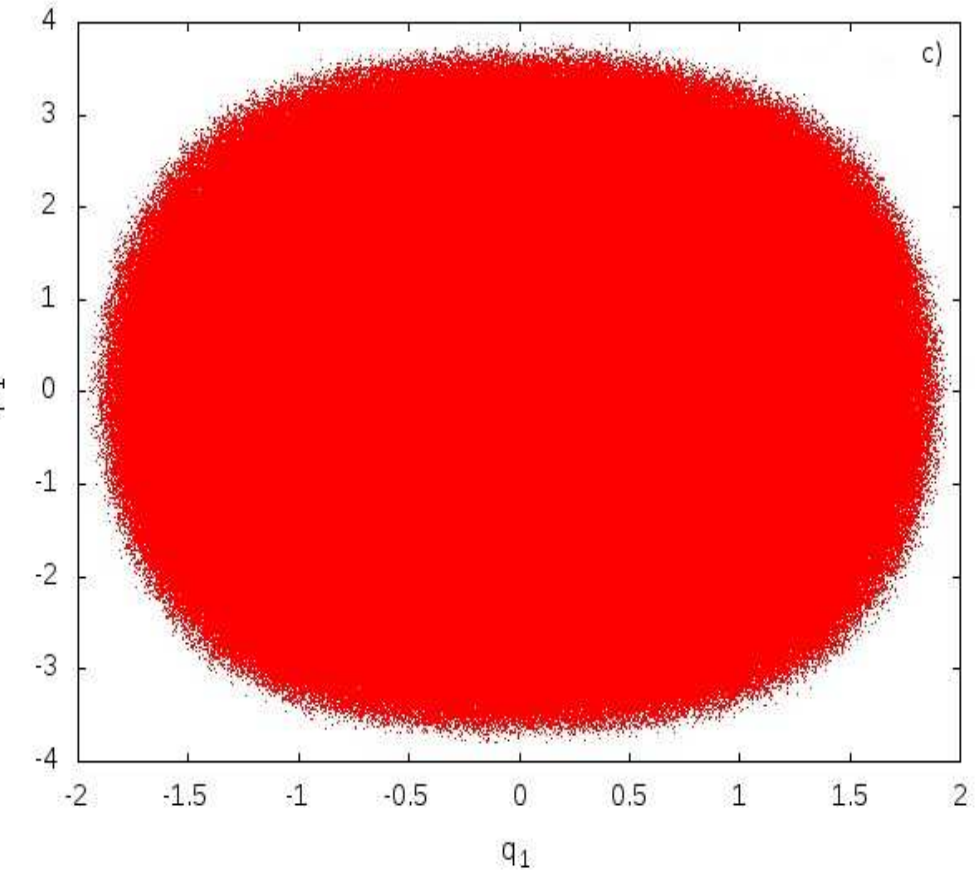

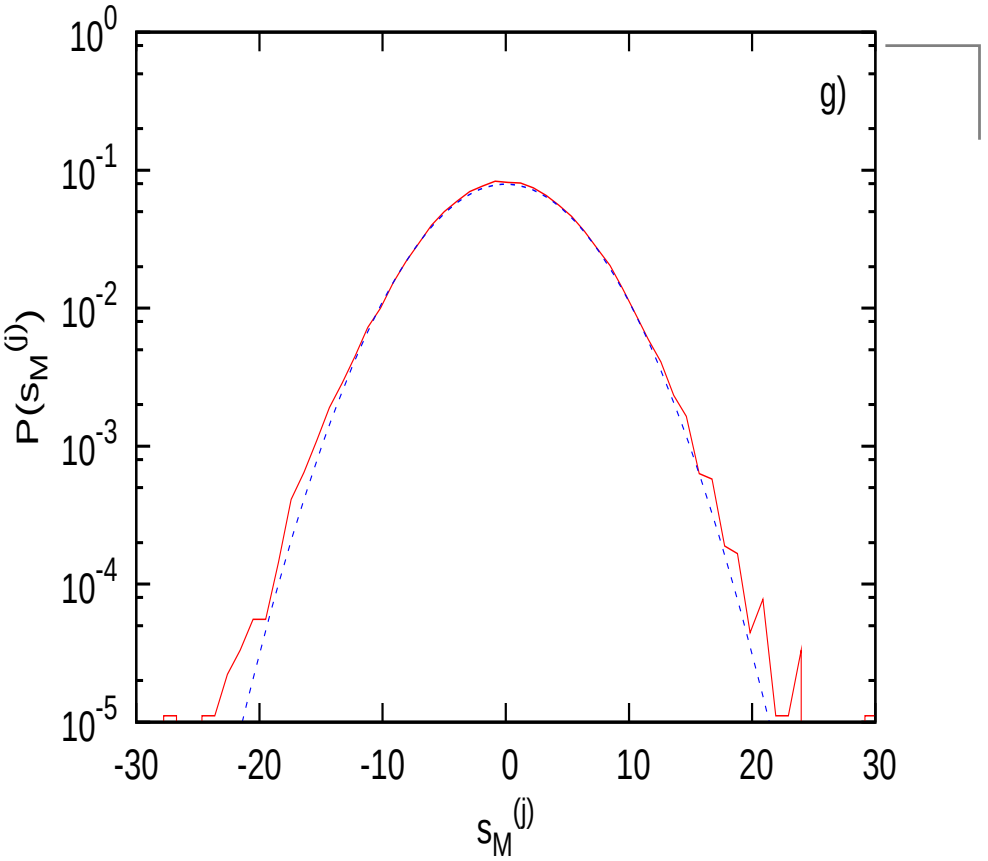

Figure 14: Left: Surface of section of the same trajectory for **total integration time** $t_f = 10^8$. **Right:** Final integration time $t_f = 10^8$ in the computations of the sums. In this case it is evident that **the distribution appears to converge to a Gaussian (q=1)**.

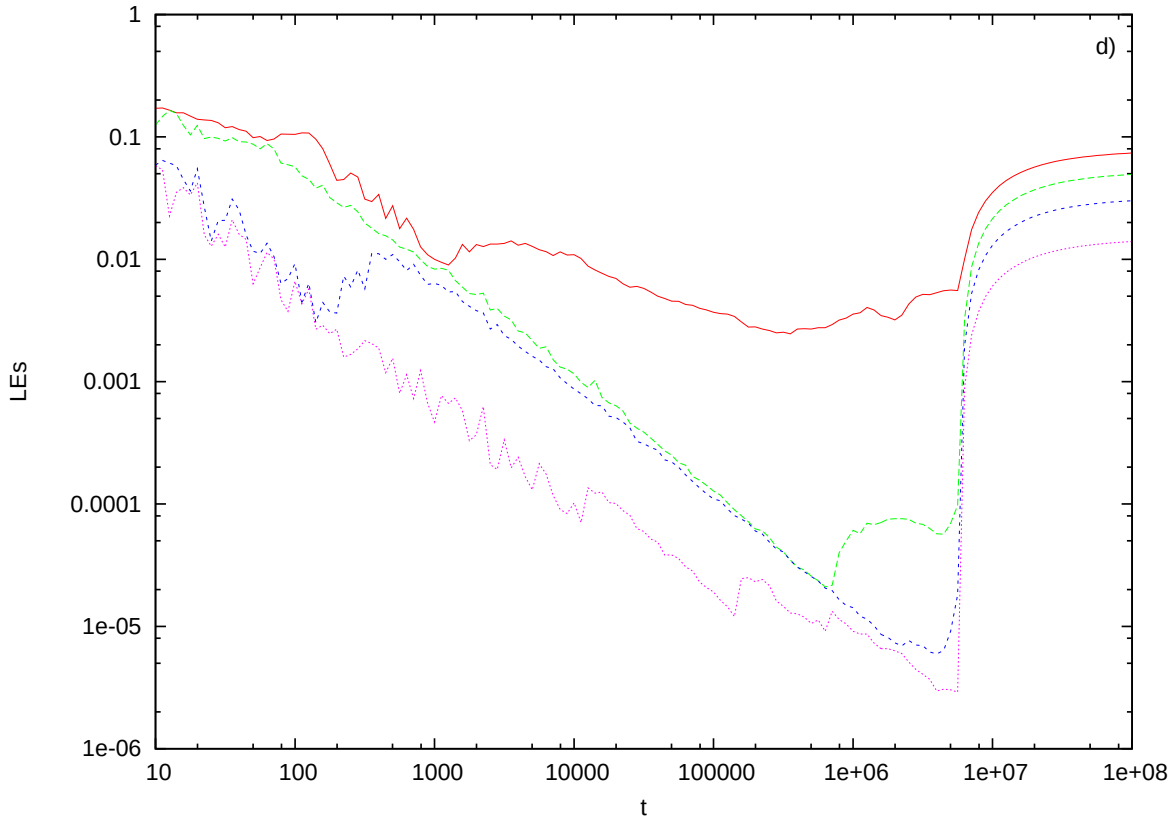

Figure 15: The 4 positive Lyapunov exponents of the previous solution integrated for a total time of $t = 10^8$. Observe the **sudden jump in their magnitude at ($t \simeq 10^7$)**, where the orbit **escapes from the region of "weak chaos" and q–Gaussian distributions** into the wider chaotic domain of **"strong chaos" where the statistics is Gaussian**.

If we perform the same study for an orbit initially located at a distance $\approx 1.086 \times 10^{-2}$ from the SPO1 and on the same surface of section we find very similar results.

More specifically, for $t_f = 10^5$, the sum distributions for this initial condition are fitted by a q–Gaussian with $q \approx 2.874$ and $\chi^2 \approx 5.48 \times 10^{-5}$. If we now increase the integration time to $t_f = 10^7$ and set $N_{\text{ic}} = 100$ and $M = 1000$, we obtain a q–Gaussian fitting with $q \approx 2$ with $\chi^2 \approx 0.00021$. Again the tails of the numerical distribution are not fitted well by a q–Gaussian distribution. Finally, for $t_f = 10^8$, time windows of length $N_{\text{ic}} = 10000$ and $M = 1000$ we get $q \approx 1.241$ with $\chi^2 \approx 0.00020$, i.e. we are even closer to a true Gaussian representing orbits that cover almost all of the available energy surface.

(c) FPU SPO2 mode under fbc

Finally, we examined the neighborhood of the SPO2 mode, which first becomes unstable at much smaller energies (i.e. $E_u^1/N \propto N^{-2}$) compared to SPO1 (i.e. $E_u^1/N \propto N^{-1}$), in the same way as low $q = 1, 2, 3, ...$ mode NNMs connected with the breakdown of FPU recurrences. Thus, we expect that near SPO2 orbits will be more weakly chaotic compared with SPO1 and hence QSS are expected to persist for even longer times.

This is indeed what happens. As figure 16 clearly shows, the dynamics in the close vicinity of SPO2 has the features of what we might call **'edge of chaos'**: Orbits trace out a kind of **"banana" shaped region** (Fig. 16(a)) in a regime of **very small (positive) Lyapunov exponents** (Fig. 16(b)). This is very different than the "figure eight" we had observed for SPO1 and the normalized sum pdfs, up to $tf = 10^{10}$!, **converge to a function that is close to a q–Gaussian**, never deviating towards a Gaussian, as shown in Figure 17.

More specifically, we take $N = 5$, $\beta = 1$, $E = 0.5$ and choose an orbit located initially at a distance $\approx 1.418 \times 10^{-3}$ from the SPO2 solution, which has just turned unstable at $E_u^1 \approx 0.4776$. As we can see on the surface of section plot of Figure 16(a), the dynamics near SPO2 **"sticks" to a type of quasiperiodic torus**, at least up to $t_f = 10^8$.

The weakly chaotic nature of the motion is plainly depicted in Figure 16(b), where we have plotted the four positive Lyapunov exponents up to $t_f = 10^9$. Note that, although they are all seen to decrease towards zero, at about $t_f > 10^9$, **the largest exponent shows a tendency to converge to a very small value of about 10^{-7}**, indicating that the orbit is chaotic and "sticky" to some quasiperiodic torus near SPO2.

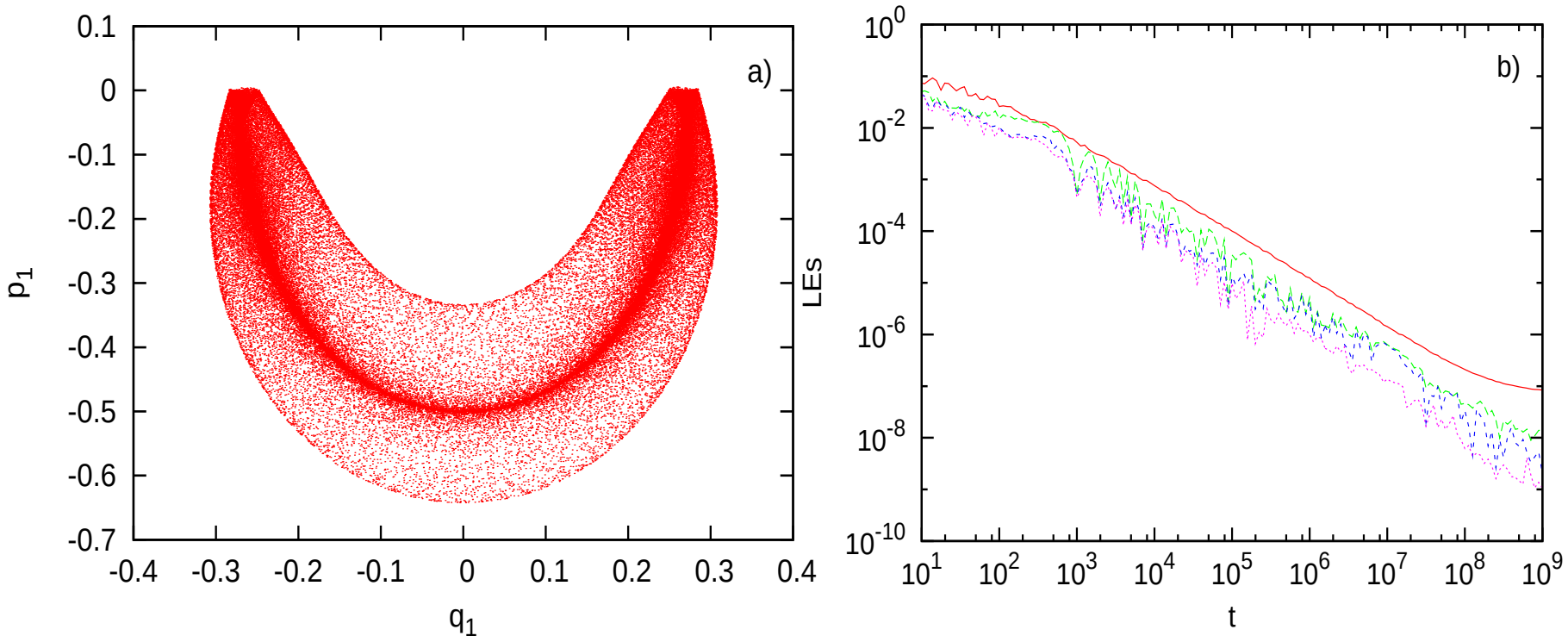

Figure 16: (a) The dynamics near SPO2 "sticks" to a quasiperiodic banana–like state, at least up to $t_f = 10^8$. The weakly chaotic nature of the motion is plainly depicted in (b), where we have plotted the four positive Lyapunov exponents up to $t_f = 10^9$. Note that, although they all decrease towards zero, at about $t_f > 10^9$, **the largest exponent shows a tendency to converge to a very small value of about** 10^{-7}, indicating that the orbit is chaotic.

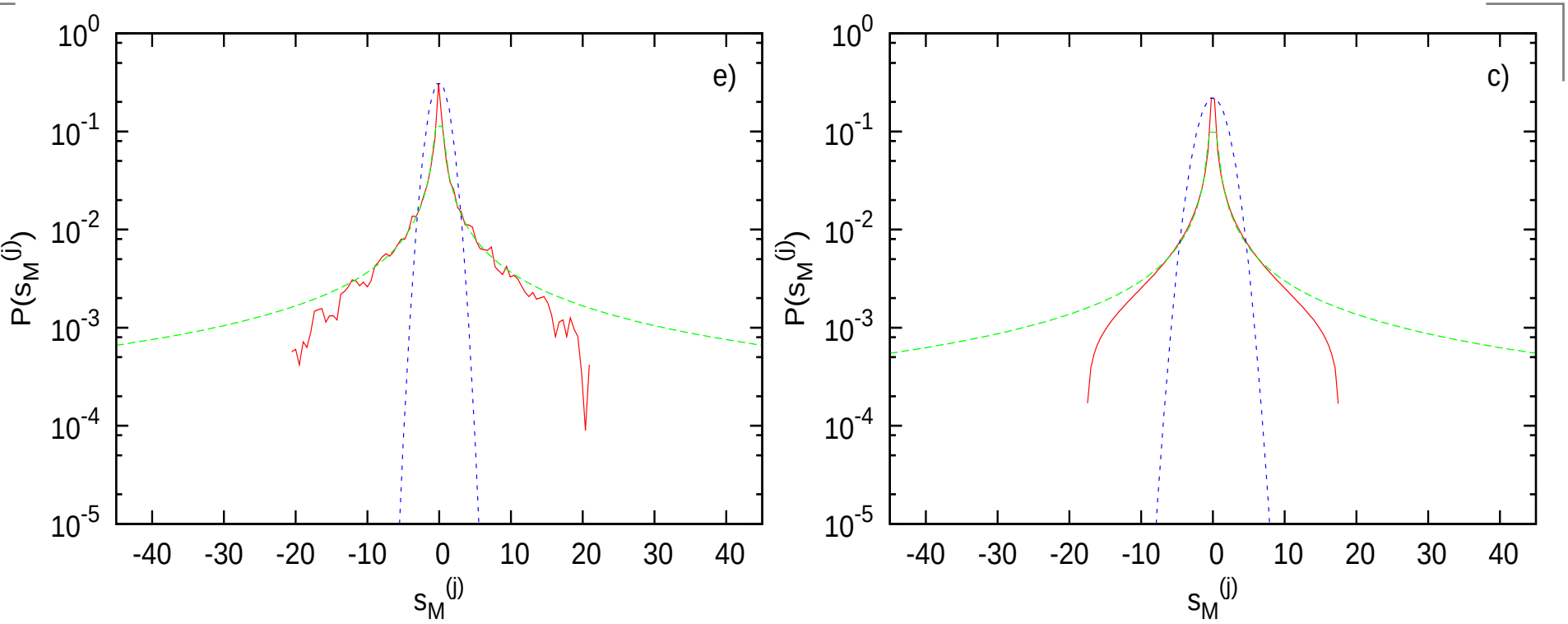

Figure 17: Left panel: The distribution of the normalized sum pdf of the orbit starting near SPO2, for a total integration time $t_f = 10^6$. Right panel: Final integration time $t_f = 10^{10}$ the normalized sum pdf has converged to a shape that closely resembles a q–Gaussian with $q \approx 2.769$ and $\chi^2 \approx 4.44 \times 10^{-5}$.

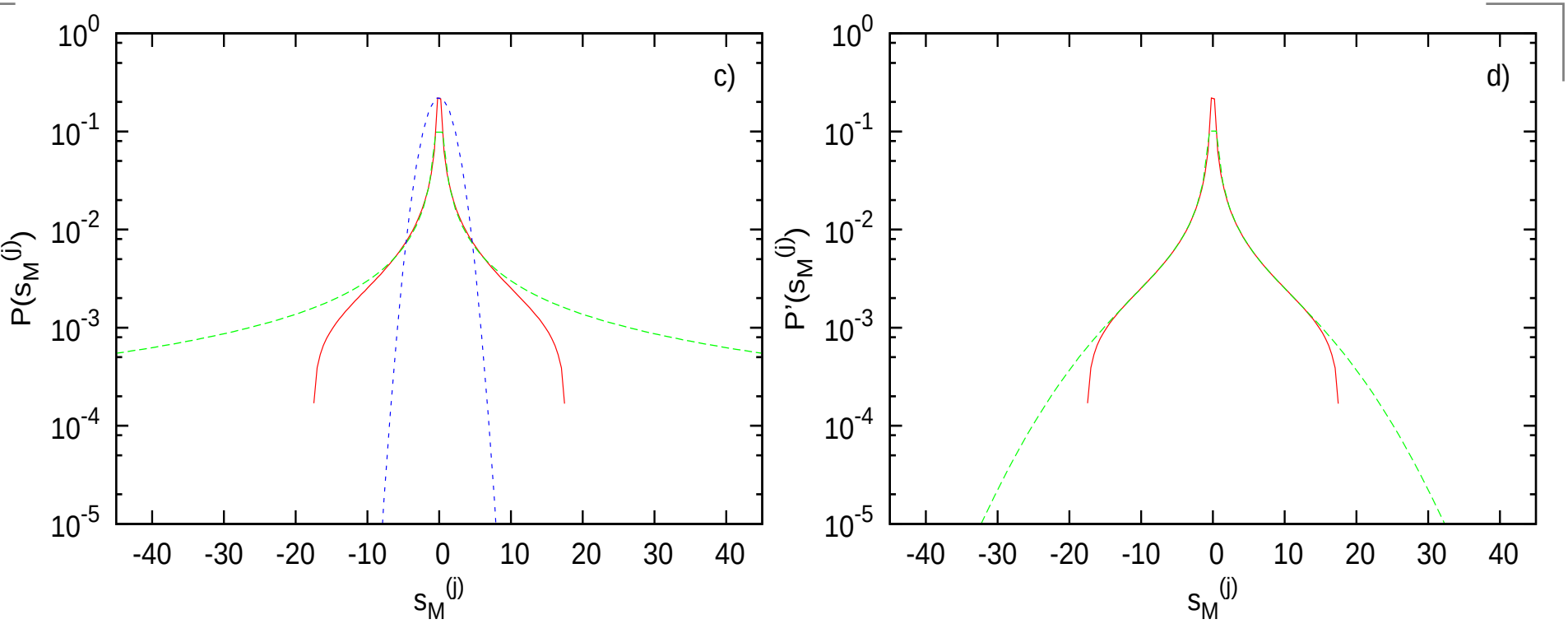

Figure 18: Left panel: The converged distribution of the normalized sum pdf of the orbit starting near SPO2, for $t_f = 10^10$. Right panel: Its analytical form is better approximated by the crossover formula (25)where $a_1 \approx 0.006$, $a_q \approx 170$ and $q \approx 2.82$ with $\chi^2 \approx 2.06 \times 10^{-6}$, than a q–Gaussian with $q \approx 2.769$ and $\chi^2 \approx 4.44 \times 10^{-5}$.

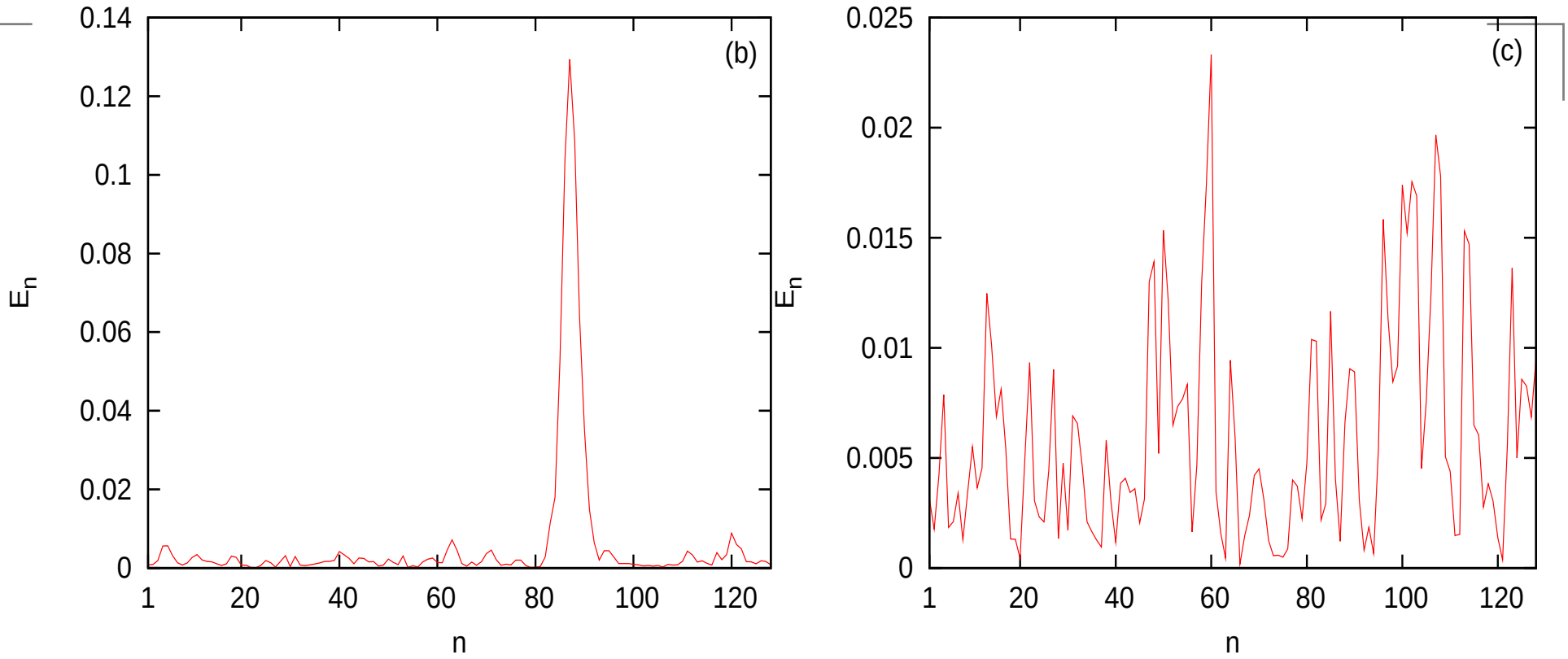

Figure 19: Plot of the instantaneous on site energy $E_n = \frac{1}{2}p_n^2 + \frac{1}{2}V(q_{n+1} - q_n) + \frac{1}{2}V(q_n - q_{n-1})$ along the $N = 128$ FPU chain with periodic boundary conditions. Panel (a) at time $t = 9 \times 10^7$ (observation of a chaotic breather), where the corresponding pdf is a q-Gaussian (q>1) and Panel (b) at time $t = 6 \times 10^8$, where the system has relaxed to an energy equipartition state and the pdf tends to a true Gaussian.

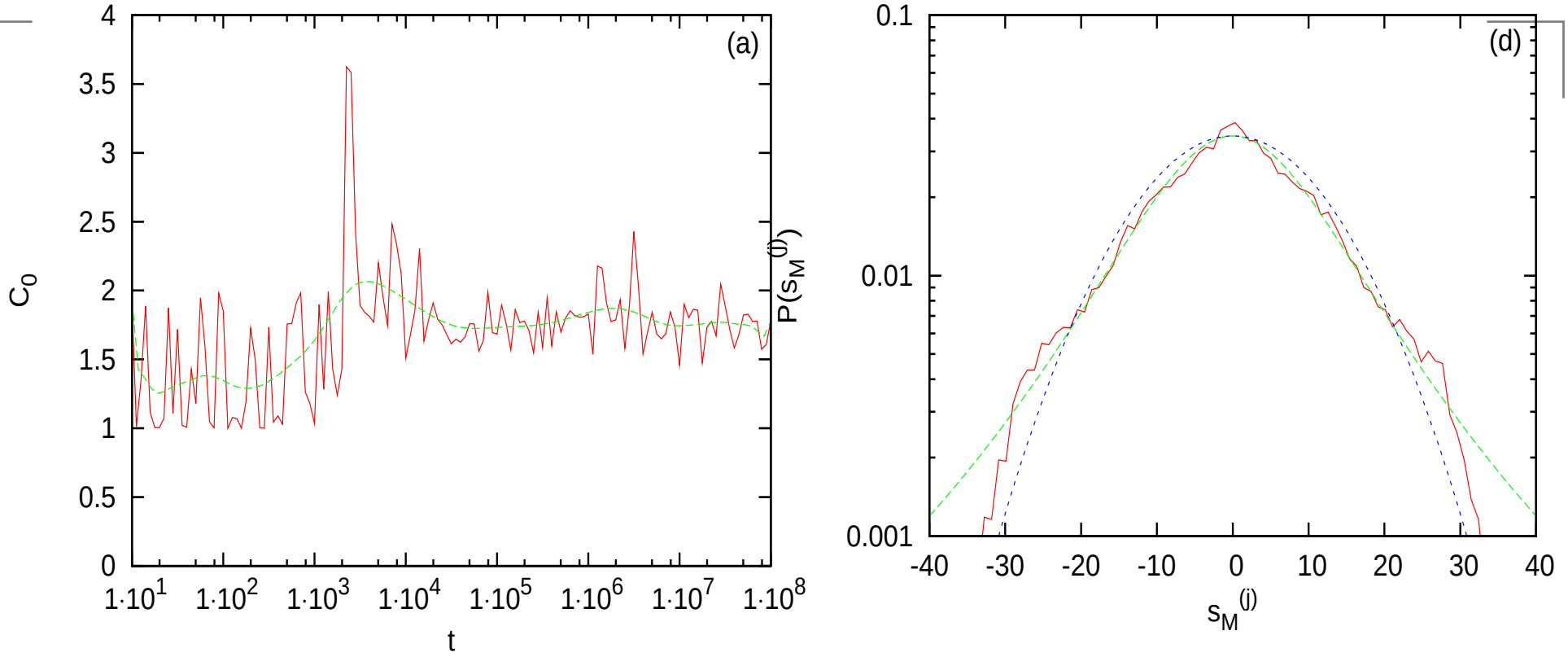

Figure 20: Panel (a) Plot of C_0 as a function of time for a perturbation of the unstable ($E = 1.5 > E_u^{\text{SPO1}} \approx 1.05226$) SPO1 mode with $\beta = 1.04$ and $N = 129$ at initial distance 2.22×10^{-7}. Plot in linear-log scale of numerical (red curve), q-Gaussian (green curve) and Gaussian (blue curve) distributions for the same initial condition and parameters as in panel (a). Panel (b) corresponds to $t_{\mathbf{f}} = 2 \times 10^6$, $N_{\text{ic}} = 5 \times 10^4$ and $M = 20$. Here, the numerical fitting gives $q \approx 1.564$ with $\chi^2 \approx 0.00014$.

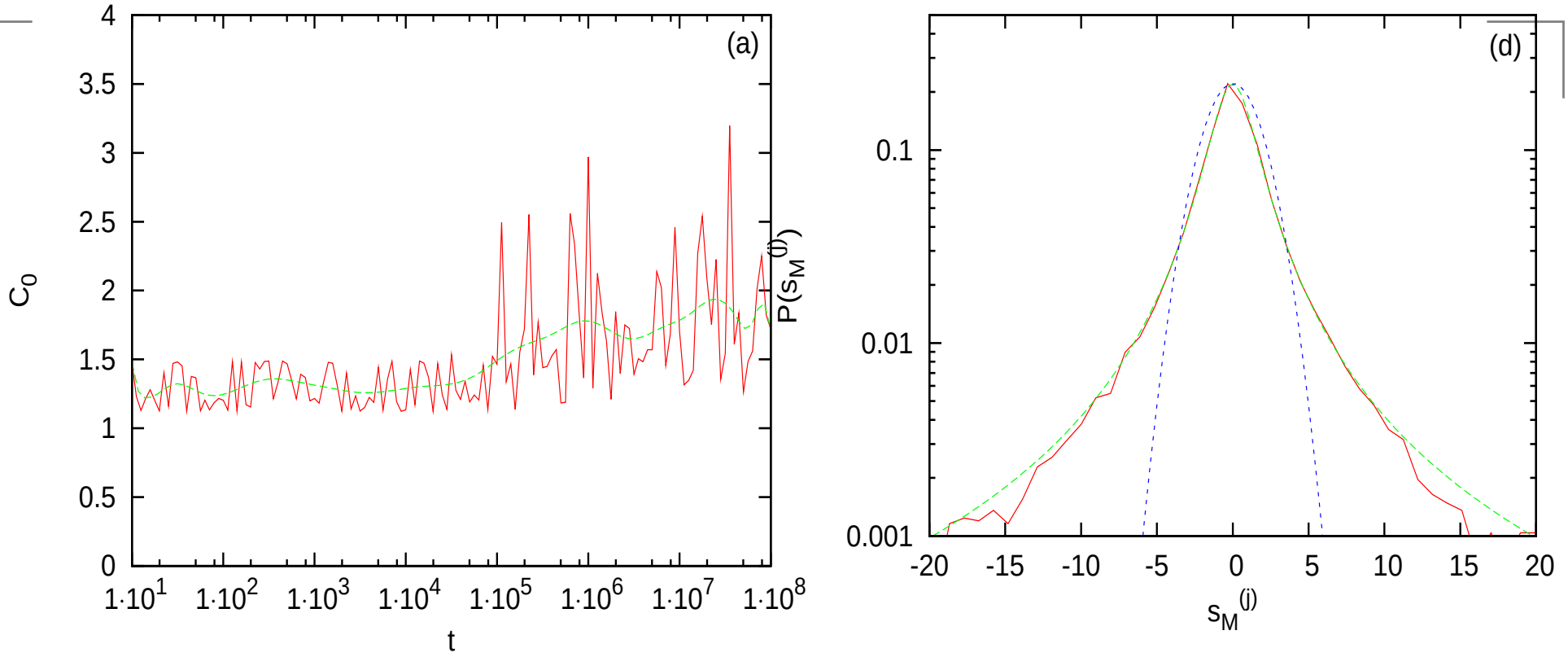

Figure 21: Panel (a) Plot of C_0 as a function of time for a perturbation of the unstable ($E = 0.1 > E_u^{\text{SPO2}} \approx 0.01279$) SPO2 mode with $\beta = 1$ and $N = 128$ at initial distance 4.09×10^{-7}. Plot in linear-log scale of numerical (red curve), q-Gaussian (green curve) and Gaussian (blue curve) distributions for the same initial condition and parameters as in panel (a). Panel (b) corresponds to $t_{\mathbf{f}} = 10^6$, $N_{\text{ic}} = 2.5 \times 10^4$ and $M = 20$. Here, the numerical fitting gives $q \approx 1.943$ with $\chi^2 \approx 0.00035$.

QSS and Dynamical Phase Transitions in a Microplasma System

We now turn our attention to another N degree of freedom Hamiltonian system of very different type than the FPU models, as **it is characterized by long range interactions of the Coulomb type** and study statistically the dynamics during the transition **from "crystalline–like" to "liquid–like"** phase (the so called "melting transition") for small energies and also **from "liquid–like" to "gas–like"** phase at higher energies. We consider a microplasma of N ions of equal mass $m = 1$ and electric charge Q in a Penning trap with electrostatic potential

$$\Phi(x, y, z) = V_0 \frac{2z^2 - x^2 - y^2}{r_0^2 + 2z_0^2} \tag{27}$$

and constant magnetic field along the z direction with a vector potential of the form

$$\mathbf{A}(x, y, z) = \frac{1}{2}(-By, Bx, 0). \tag{28}$$

The system is described by the Hamiltonian

$$\mathcal{H} = \sum_{i=1}^{N} \left\{ \frac{1}{2m}(\mathbf{p}_i - q\mathbf{A}(\mathbf{r}_i))^2) + Q\Phi(\mathbf{r}_i) \right\} + \sum_{1 \le i < j \le N} \frac{Q^2}{4\pi\epsilon_0 r_{ij}} \tag{29}$$

Here $\mathbf{r_i}$ is the position of the ith ion, r_{ij} is the Euclidean distance between the ith and jth ions and ϵ_0 is the vacuum permittivity. The ions are subjected to a **harmonic confinement in the z direction** with frequency

$$\omega_z = \sqrt{\frac{4QV_0}{m(r_0^2 + 2z_0^2)}} \tag{30}$$

while, in the perpendicular direction, they rotate with frequency $\omega_c = QB/m$. Thus, in a frame rotating around the z axis with Larmor frequency $\omega_L = \omega_c/2$, the ions are subjected to a **harmonic confinement** with frequency $\omega_x = \omega_y = \sqrt{\frac{\omega_c^2}{4} - \frac{\omega_z^2}{2}}$ in the direction perpendicular to the magnetic field. In the rescaled time $\tau = \omega_c t$, position $\mathbf{R} = \mathbf{r}/a$ and energy $H = \frac{\mathcal{H}}{m\omega_c^2 a^2}$ with $a = \left(\frac{Q^2}{4\pi\epsilon_0 m\omega_c^2}\right)^{\frac{1}{3}}$, the Hamiltonian (29) describing the motion of the N ions takes the form

$$H = \sum_{i=1}^{N}\Big[\frac{1}{2}\mathbf{P}_i^2\Big] + \sum_{i=1}^{N}\Big[\Big(\frac{1}{8} - \frac{\gamma^2}{4}\Big)(X_i^2 + Y_i^2) + \frac{\gamma^2}{2}Z_i^2\Big] + \sum_{i<j}\frac{1}{R_{ij}} = E \tag{31}$$

where E is the total conserved energy of the system, $\mathbf{R}_i = (X_i, Y_i, Z_i)$ and $\mathbf{P}_i = (P_{X_i}, P_{Y_i}, P_{Z_i})$ are the positions and momenta in $\mathbb{R}^3$, R_{ij} is the Euclidean distance between different ions i, j given by

$$R_{ij} = \sqrt{(X_i - X_j)^2 + (Y_i - Y_j)^2 + (Z_i - Z_j)^2} \tag{32}$$

and $\gamma = \omega_z/\omega_c$. The ions perform bounded motion under the condition that

$$0 < |\gamma| < \frac{1}{\sqrt{2}}. \tag{33}$$

The trap is called prolate if $0 < |\gamma| < \frac{1}{\sqrt{6}}$, isotropic if $|\gamma| = \frac{1}{\sqrt{6}}$ and oblate if $\frac{1}{\sqrt{6}} < |\gamma| < \frac{1}{\sqrt{2}}$. Thus, **the motion is quasi 1–dimensional in the limit** $\gamma \to 0$ and quasi 2–dimensional in the limit $\gamma \to 1/\sqrt{2}$. The Z direction is a symmetry axis and hence, the Z component of the angular momentum $L_Z = \sum_{i=1}^{N} X_i P_{Y_i} - Y_i P_{X_i}$ is conserved. We suppose, from now on $L_Z = 0$) and that the motion is studied in the Larmor rotating frame.

Recent results demonstrate **the occurrence of dynamical regime changes** when the system is in a prolate **quasi 1–dimensional configuration ($\gamma = 0.07$)**. More specifically, in the **lower energy regime**, a transition from a "crystalline–like" to a "liquid–like" behavior is observed, called the "melting phase". This is not associated with a sharp increase of the temperature at some critical energy and the positive Lyapunov exponents attaining high values. Thus, it appears that there is no clear "macroscopic" approach for identifying and studying the "melting" process of the microplasma system in detail.

Using the **Smaller Alignment Index (SALI) method** to study the local dynamics, it was discovered that **there exists an energy range E_{mt} of weakly chaotic behavior**, i.e. $E \in E_{\text{mt}} = (2, 2.5)$, where **the positive Lyapunov exponents are very small** and SALI exhibits a stair–like decay to zero with varying decay rates, due to the presence of long lived "sticky" orbits near the boundaries of resonance islands.

Thus, we set $\gamma = 0.07$ and consider a prolate trap giving rise to **quasi 1–dimensional motion** for the case of $N = 5$ **ions**. For these parameters, the minimum energy for the ions to start moving around their equilibrium positions is $E_0 \approx 1.8922$.

We first study **the "melting transition"**, as the energy of the Hamiltonian (31) increases above E_0, from the viewpoint of probability distributions associated with chaotic trajectories. Based on the results of the previous sections, we expect to find q–Gaussians with $1 < q < 3$ in the vicinity of E_{mt} where the positive Lyapunov exponents $\lambda_i,\ i = 1, \ldots, 3N$ are quite small compared to the maximum values they can attain. This is also expected since in the interval E_{mt} the orbits stick to the boundaries of islands, at the so called **"edge of chaos"** [Tsallis, 2009].

Indeed, in Figure 22, we apply our statistical analysis to the microplasma system, taking $N_{\text{ic}} = 1000$, $M = 1000$, $t_f = 2 \times 10^7$ as integration time for our orbits and **using as an observable the quantity** $\eta(t) = X_1(t)$, i.e. the first component of the position $\mathbf{R}_1$ of the first ion. We find that, in the energy range of the "melting transition", the values of the entropic parameter of the q–Gaussian distribution (14) exhibiit **a maximum well above** $q = 1$, indicating that the statistics is not Gaussian. Rather, a q–Gaussian is detected, which persists up to about $E = 4.5$.

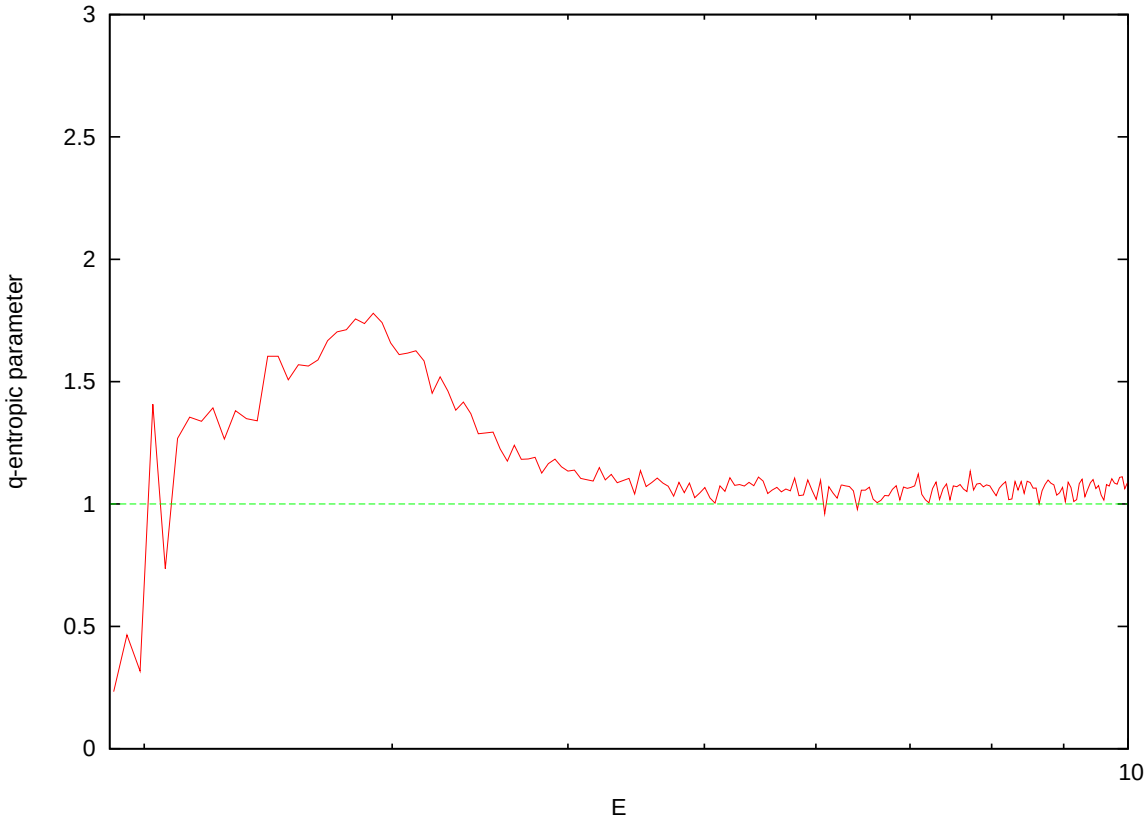

Figure 22: Plot of the q–entropic parameter as a function of the energy E of the microplasma Hamiltonian (31) for $\gamma = 0.07$ (prolate trap) and $N = 5$ ions. In this plot, we have used $N_{\text{ic}} = 1000$ and $M = 1000$. We have also plotted the line at $q = 1$ for reference to the entropic parameter of the Gaussian distribution.

Finally, we study a **second transition from "liquid–like" to "gas–like"** behavior, where the system is "weakly chaotic" at higher energies, where the biggest Lyapunov exponents decrease towards zero according to the equation [see Gaspard, 2003]

$$\mathrm{LE}_1 \sim \left\langle \frac{N^2}{R_{ij}^3} \right\rangle \sim N \frac{(\ln T)^{1/2}}{T^{3/4}} \tag{34}$$

where T is defined as $T = \frac{k_B \mathcal{T}}{m\omega_c^2 a^2}$, with $\mathcal{T}$ being the temperature of the system. This formula represents the asymptotic power law decay of the biggest Lyapunov exponent for sufficiently high energies (well above its peak at $E \approx 6$), see Figure 20(a).

As Figure 20(b) shows, the q indexes of the distributions are **well above unity for** $E \in (30, 200)$ indicating that in this range a significant dynamical change occurs. The energy increase drives the system to a more organized state favoring the kinetic part rather than the Coulomb part and leading to a regime characterized by few rare particle encounters, much like in an "ideal gas".

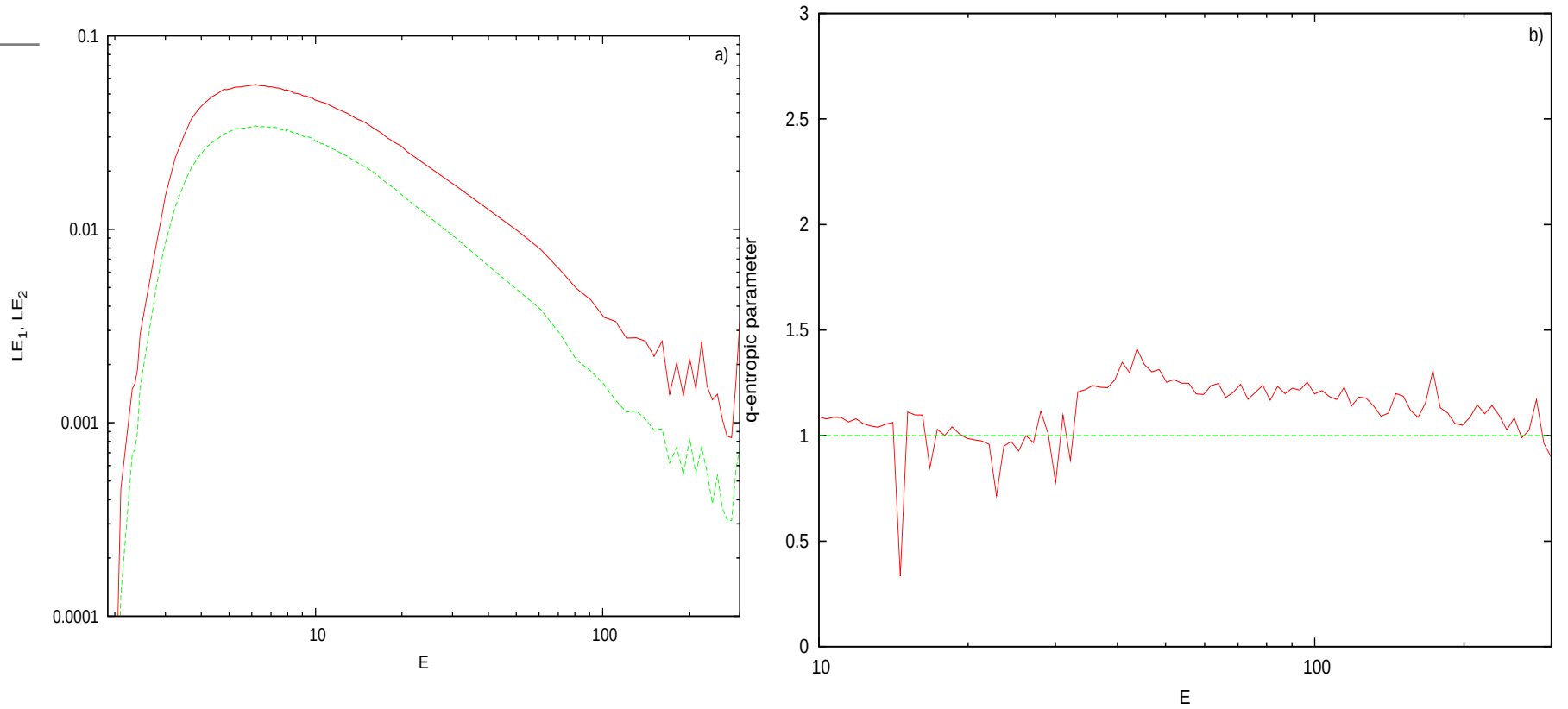

Figure 20: Panel a) Plot of the two biggest positive Lyapunov exponents (LE_1 with red color and LE_2 with green color) as a function of the energy E in log–log scales. We observe that, after their peak values at $E \approx 6$, both of them decay to zero according to the formula (34). Panel b) Plot in log–linear scales of the q–entropic parameter as a function of E for $\gamma = 0.07$ (prolate trap) and $N = 5$ ions. In this plot, we have used $N_{\mathrm{ic}} = 1000$ and $M = 1000$.

Conclusions

1. It appears that, at the **"edge of chaos"** located at the boundaries of islands of quasiperiodic motion of **Hamiltonian systems**, probability density functions (pdfs) of sums of chaotic variables, are **well approximated by q–Gaussians**.

2. These q–Gaussians are in fact **Quasi–Stationary States** (QSS) which **last for long times**, passing through **different stages** during which the **central part retains its q–Gaussian form**. The tails, however, generally **shift downward** as the pdf tends to the **expected Gaussian ($q = 1$)**.

3. In some cases, when one is **very close to the "edge of chaos"**, it is possible to find that the orbits **converge to a specific QSS**, whose pdf is **close to a q–Gaussian**, but is **better approximated** by a function recently proposed in [Tsallis and Tirnakli, 2010].

5. QSS approximated by q–Gaussians can be used to **identify energy ranges** where **dynamical transitions** (like "melting" or "evaporation") occur in certain long range Hamiltonian systems (like the microplasma model) under "weakly chaotic" conditions.

4. These results are also observed in **low–dimensional conservative maps** and seem to be **independent of the number of degrees of freedom** in the case of Hamiltonian systems.

References

1. Tsallis, C. [2009], “Introduction to Nonextensive Statistical Mechanics: Approaching a Complex World”, *Springer, New York*.

2. Umarov, S., Tsallis, C. and Steinberg, S. [2008], “On a q–Limit Theorem Consistent with Nonextensive Statistical Mechanics”, *Milan J. of Math.*, **76**, 307 – 328.

3. Antonopoulos, C., **Bountis, T.** and Basios, V. [2010], “Quasi–Stationary States in Multidimensional Hamiltonian Systems”, preprint submitted for publication.

4. Ruiz Lopez G., **Bountis, T.** and Tsallis, C. [2010], “Time–Evolving Ststistics of Chaotic Orbits in Conservative Maps in the Spirit of the Central Limit Theorem”, preprint submitted for publication.

5. Tsallis, C. and Tirnakli, U. [2010], “Nonadditive Entropy and Nonextensive Statistical Mechanics – Some Central Concepts and Recent Applications”, *J. of Phys.: Conf. Ser.*, **201**, 012001.

6. Leo, M. and Leo, R. A. and Tempesta, P. [2010], “Thermostatistics in the Neighborhood of the π–mode Solution for the Fermi–Pasta–Ulam β System: From Weak to Strong Chaos”, *J. of Stat. Mech.: Th. & Exp.*, **04**, pp. 04021.

7. Antonopoulos, Ch., **Bountis, T.** and Skokos, Ch., [2006],“Chaotic Dynamics of N–Degree–of–Freedom Hamiltonian Systems”, *International Journal of Bifurcation and Chaos*, vol.**16**(6), 1777-1793 , June 2006.

8. Antonopoulos, Ch. and **Bountis, T.**, [2006], “Stability of Simple Periodic Orbits and Chaos in an FPU Lattice”, PRE**73**, 056206, 1-8 (2006).